

Foreground analysis of the *WMAP* three-year data with FASTICA

M. Bottino^{1,2*}, A. J. Banday², D. Maino¹

¹ *Dipartimento di Fisica, Università di Milano, Via Celoria 16, I-20133, Milano, Italy*

² *Max-Planck Institute für Astrophysik, Karl-Schwarzschild Str. 1, D-85748, Garching, Germany*

18 December 2018

ABSTRACT

We present an analysis of the foreground emission present in the *WMAP* 3-year data as determined by the method of Independent Component Analysis. The *WMAP* data averaged at each frequency are used together with the standard foreground emission templates as inputs to the FASTICA algorithm. The returned coefficients can be interpreted as coupling coefficients between the *WMAP* data and foreground templates. These results are then used to infer the spectral behaviour for three foreground components – synchrotron, anomalous dust-correlated emission and free-free. For the first two components, we find values consistent with previous results although slightly steeper. We confirm the inconsistency in the scaling between the H α template and free-free emission at K- and Ka-bands where an electron temperature of ~ 4000 K is indicated. We also see evidence of significantly flatter spectral behaviour to higher frequencies than expected theoretically and previously noted by Dobler et al. (2008a), but only when analysing the *Kp2* sky coverage.

We further apply FASTICA ‘iteratively’, using data pre-cleaned using foreground templates scaled to the *WMAP* frequencies by coupling coefficients determined by a prior FASTICA analysis. This multi-frequency analysis allows us to determine the presence of residual foreground emission not traced by the templates. We confirm the existence of a component spatially distributed along the Galactic plane and particularly enhanced near the center (the ‘*WMAP* haze’). This emission is less extended when using the *WMAP* K-Ka data as the synchrotron template confirming that it can be considered a better template for foreground cleaning of the *WMAP* data. However its use complicates the physical interpretation of the nature of the foreground emission and residuals since it contains a mixture of several, physically distinct emission mechanisms.

The good agreement between the extracted CMB component and previous results, as well as the low amplitude of residual foreground emission make FASTICA a viable tool to infer foreground emission properties, via template fitting, and the CMB amplitude.

Key words: methods: data analysis – techniques: image processing – cosmic microwave background.

1 INTRODUCTION

Measurements of the Cosmic Microwave Background (CMB) provide cosmological information by probing the early universe some 380,000 years after the Big Bang. However their precision is limited by the contamination of the cosmological signal due to emission from local astrophysical sources such as our own Galaxy. In particular the Galactic contamination arises

* E-mail: bottino@mpa-garching.mpg.de

from three well-understood processes: synchrotron emission, free-free emission (or *thermal bremsstrahlung*) and thermal dust emission. In addition, there appears to be an enhanced dust correlated emission at microwave wavelengths that is inconsistent with the thermal mechanism, and the exact nature of which is still open to debate. Theoretically, these components can be distinguished on the basis of their own spectral properties and spatial distribution. The best window for observing the temperature anisotropies lies close to 70 GHz, where the integrated diffuse foreground emission seems to display a minimum. This has permitted accurate mapping of the CMB intensity pattern, without the need to excise too much sky coverage from the analysis due to these foregrounds (except in regions near to the Galactic plane and associated with bright point sources). However, to reach the accuracy required for precision cosmology ($\sim \mu\text{K}$), component separation techniques and/or foreground cleaning methods are needed.

A component separation technique is one that attempts to decompose multi-frequency input data into separate physical emission components, one of which, for our purposes, must be the CMB. However, the technique may not be successful particularly in regions of the sky where the foreground spectral dependencies are complex, or where the physical emissions have complex morphology and are well-mixed. A foreground cleaning method in the context of this paper simply attempts to generate a map of the CMB as clean of foreground emission as possible, with no concern for the detailed separation of the foreground emission into physical components. It should be clear that a component separation algorithm may have limited success, providing an adequate reconstruction of the CMB but not of the foreground emission, then effectively constituting a foreground cleaning method.

In this paper we will consider the detailed application of one technique – *Independent Component Analysis* (ICA) – to data from the *WMAP*¹ satellite, focusing our attention on the properties of diffuse Galactic foregrounds at high and intermediate latitude as traced by specific templates of the emission. Of course, FASTICA is only one of a number of methods that have been developed for the application to data at microwave wavelengths in order to (at least) extract a map of the CMB sky with minimal foreground residuals. An inexhaustive list of other techniques applied to the *WMAP* data includes linear combination methods (Bennett et al. 2003; Tegmark et al. 2003; Park et al. 2007), WIFIT (Hansen et al. 2006), FGFit (Eriksen et al. 2006), SMICA (Patanchon et al. 2005) and CCA (Bonaldi et al. 2007). The *WMAP* team has also made use of the Maximum Entropy Method (MEM) (Bennett et al. 2003; Hinshaw et al. 2007) to study the detailed properties of the Galactic foregrounds. However, since MEM is not able to produce a CMB map that is easy to use for cosmological analyses, the *WMAP* data was cleaned from foregrounds by applying a template fitting algorithm – essentially a cross-correlation method also used by Davies et al. (2006) to study regional variations in the foreground emission.

A general summary of the paper is as follows. We first provide a simple introduction to ICA and describe the use of templates of foreground emission in such an analysis, making a comparison to more standard template fitting techniques. We then describe the data used in this paper for the foreground analysis. Then we calibrate the performance of the method using Monte Carlo simulations and by comparison to the simpler template based method. Sections 5 and 6 then attempt to improve our knowledge of the spectral and physical properties of the foreground components based on the scaling properties of the templates. An assessment of the efficiency of the method is then afforded by studying the power spectrum of the cleaned CMB data, whilst a final iterative application of ICA attempts to improve the removal of foreground contamination from the data. Section 9 summarises our main conclusions.

2 FASTICA AND ITS USE FOR FOREGROUND COMPONENT STUDIES

ICA is a *blind* component separation method: it works without any knowledge about the spectral and spatial properties of the components to be recovered. A particular application of this method is FASTICA as originally proposed by Hyvärinen (1999); Hyvärinen & Oja (2000) and applied to the analysis of CMB total intensity data in Maino et al. (2002) and more recently to polarization in Maino et al. (2002) and Baccigalupi et al. (2004).

The component separation problem is formalized assuming that the sky radiation at a given frequency ν can be described as a linear combination of N different physical processes whose frequency and spatial dependencies can be factorized into two terms:

$$\tilde{x}(\mathbf{r}, \nu) = \sum_{j=1}^N \bar{s}_j(\mathbf{r}) f_j(\nu). \quad (1)$$

Generally the radiation is observed by a combination of an optical system and a M-channel measuring instrument. In what follows, we will assume that the observations can then be described as the convolution of the sky signal with a frequency dependent azimuthally symmetric beam response and a bandpass $t_\nu(\nu')$ (the frequency response of the channel) which is effectively a delta function. The former assumption will generally be violated, but for *WMAP* the effect of multiple observations of a given point on the sky with the detectors in different relative orientations (due to the satellite scan pattern)

¹ *Wilkinson Microwave Anisotropy Probe*

results in an effectively symmetric beam. This may not be the case for the *Planck* satellite. The latter assumption can also be improved on by defining an effective frequency for a given detector depending on the spectral behaviour of the impinging radiation. Nevertheless, with our simplifying assumptions we can define the scaling coefficients $a_{\nu j} = f_j(\nu)$, and construct the relevant $M \times N$ mixing matrix \mathbf{A} . If we introduce the instrumental noise ϵ , and we assume that the beam function is frequency independent $B(\mathbf{r}, \nu) = B(\mathbf{r})$, the observed signal for each position r is expressed by

$$\mathbf{x}(\mathbf{r}) = \mathbf{A}\bar{\mathbf{s}}(\mathbf{r}) * B(\mathbf{r}) + \epsilon(\mathbf{r}) = \mathbf{A}\mathbf{s}(\mathbf{r}) + \epsilon(\mathbf{r}), \quad (2)$$

where \mathbf{x} and ϵ are vectors with M rows, and the star represents the convolution of the beam PSF with the sky signals $\bar{\mathbf{s}}$, indicated simply as \mathbf{s} afterward.

The ICA approach then estimates both the matrix \mathbf{A} and the vector \mathbf{s} from the data \mathbf{x} by assuming that

- the sources \mathbf{s} are random independent processes on the map
- the components of the vector \mathbf{s} with at most one exception have non-Gaussian distributions.

The problem is solved by finding a linear transformation \mathbf{W} so that the components of the transformed vector $\mathbf{y} = \mathbf{W}\mathbf{x}$ are independent. Using the *Central Limit Theorem* the independence is achieved maximizing the non-Gaussianity of the variables. This corresponds to the maxima of their *neg-entropy* which in the FASTICA implementation is generally approximated by three non-linear functions, i.e. $p(u) = u^3$, $t(u) = \tanh(u)$ and $g(u) = u \exp(-u^2)$ where u are the principal component projected data (Hyvärinen 1999; Hyvärinen & Oja 2000). These functions depend on the statistics of the independent signals which are assumed to be unknown. Generally, p , which corresponds to the kurtosis, should be used for sub-Gaussian components but it is strongly sensitive to outliers in the distributions; g is for super-Gaussian signals while t is a general purpose function (Hyvärinen 1999). Although FASTICA is a non linear algorithm, the returned components are defined as linear combinations of the input data, whose weights are the elements of the matrix \mathbf{W} :

$$y_j = \sum_{i=1}^M w_{ij} x_{\nu_i}. \quad (3)$$

Once the matrix \mathbf{W} is determined, the independent components are recovered via the relation:

$$x_{\nu_i} = \sum_{j=1}^N w_{ij}^{-1} y_j \quad (4)$$

with $i = 1, \dots, N$.

FASTICA has been utilised in component separation studies for both the *COBE*-DMR and *WMAP* multi-frequency observations of the microwave sky in Maino et al. (2002) and Maino et al. (2006) respectively. However, in general it has been found that the foreground components returned by the method are not optimal – a fully reliable component separation is not achieved. Nevertheless, one of the output maps of the analysis can, in general, be associated explicitly and robustly with the CMB signal. In an alternative approach, Maino et al. (2002) proposed the analysis of a single microwave sky map in combination with observations at wavelengths where only single foreground physical emission processes dominate. These various foreground templates are considered to be representative models for the morphology of the foreground emission at that wavelength (see section 3 for details of the templates used in this analysis), except for a scale-factor to be determined. Application of the FASTICA algorithm then provides information on foreground emission, not directly from the spectral properties of the reconstructed and ambiguous Galactic components, but from the recovered CMB component. Referring to Eq. 2, the reconstructed CMB component is defined as a weighted linear combination of the input data, namely the microwave sky map and putative templates of Galactic emission. Those coefficients associated with the foreground templates define the effective contamination of the CMB anisotropy signal by each foreground. After normalising the weights so that the factor associated with the microwave sky map is unity, we can then interpret the modified template weights as correlation coefficients between the foregrounds and a given channel of the microwave data. Therefore with FASTICA-derived CMB sky maps at different frequencies, we can derive the frequency dependence of the coupling coefficients associated with a given template or physical foreground component.

However, for such an analysis it is necessary to focus attention on the high and intermediate latitudes for two reasons. Firstly, it is likely that the physical conditions within the Galactic plane are different to those at higher latitudes, so that the assumption that the templates can be scaled to a given wavelength by a single factor (or spectral index) is almost certainly invalidated, thus a global FASTICA analysis will be compromised. Secondly, the complex morphology of the Galactic plane results in non-negligible correlations between the different emission mechanisms, thus violating one of the assumptions of the ICA approach.

Such an analysis is then directly analogous to the simple template fitting scheme commonly used in the field. Therefore, we also utilise the technique here as a convenient point of reference for our FASTICA results. In general, the cross-correlation measure, α , between a data vector \mathbf{d} and a template vector \mathbf{t} can be measured by minimising:

$$\chi^2 = (\mathbf{d} - \alpha \mathbf{t})^T \cdot \mathbf{M}_{SN}^{-1} \cdot (\mathbf{d} - \alpha \mathbf{t}) = \tilde{\mathbf{d}}^T \cdot \mathbf{M}_{SN}^{-1} \cdot \tilde{\mathbf{d}} \quad (5)$$

where \mathbf{M}_{SN} is the covariance matrix including both signal and noise for the template-corrected data vector $\tilde{\mathbf{d}} \equiv \mathbf{d} - \alpha\mathbf{t}$. In the case of N different foreground components, we have the simple system of linear equations $\mathbf{A}\mathbf{x} = \mathbf{b}$, where

$$\begin{aligned} A_{kj} &= \mathbf{t}_k^T \cdot \mathbf{M}_{SN}^{-1} \cdot \mathbf{t}_j, \\ b_k &= \mathbf{t}_k^T \cdot \mathbf{M}_{SN}^{-1} \cdot \mathbf{d}, \\ x_k &= \alpha_k. \end{aligned} \tag{6}$$

The correlation method can also be extended to include various constraints on the data, eg. fixed dust or free-free spectral indices. This is the case described by Hinshaw et al. (2007) in the analysis of the 3 year data of *WMAP* but we impose no such constraints here.

Once the scaling factors are computed they can be used to clean the *WMAP* data from the estimated Galactic contaminations. The residuals then provide another characterization of the accuracy of the cleaning process. Indeed, residual foreground components are expected that are not well correlated with the adopted foreground templates. They are most easily interpreted as a consequence of the main limitation of FASTICA as currently applied, namely the de-facto assumption of a fixed spectral index for each physical foreground component over the analysed sky coverage. We will show that an ‘iterative’ application of the FASTICA algorithm to multi-frequency pre-cleaned microwave data can provide additional insight into such residuals and an additional estimate of the CMB component. The outcome of such an iterative stage will include an improved CMB sky map, plus component maps that represent foreground residuals, although it is unlikely that they can be unambiguously assigned to specific physical components.

3 DATA USED IN THE ANALYSIS

The current analysis seeks to clean the *WMAP* data from the main Galactic foreground emissions by applying the FASTICA algorithm to the observed *WMAP* sky signal at each frequency together with appropriate templates for each component. The current implementation of the FASTICA algorithm assumes that each input sky map has the same spatial resolution. Thus we perform our analysis on sky maps convolved from their original resolution to an effective 1° Gaussian beam. Since regions close to the Galactic plane are the most seriously contaminated by foregrounds and the spectral and spatial nature of the integrated emission is complex, we exclude them according to the *Kp2* and *Kp0* masks provided by the *WMAP* team (Bennett et al. 2003). The Galactic part of the masks as well as the point-source exclusion regions are considered sufficient and no modifications are made.

3.1 *WMAP* data

The *WMAP* satellite (Hinshaw et al. 2007) observes the sky with ten so-called differencing assemblies (DAs), with frequency dependent resolution of approximately 0.23° to 0.93° . The frequency ranges from ~ 23 GHz (K-band) up to ~ 94 GHz (W-band): there are two channels in the Q- and V-bands, and four channels in the W-band whilst there is only one channel at each of the K- and Ka-bands. The corresponding sky map data are available on the LAMBDA website² in a HEALPix³ pixelisation scheme, with a pixel resolution parameter of $N_{side} = 512$.

We have smoothed each of the sky maps to an effective resolution of 1° (initially deconvolving the azimuthally symmetric beam profile for each DA), then we have combined the maps in the Q-, V- and W-bands using a simple average over the corresponding DAs in order to generate a single map for each frequency band. The effective central frequency of each DA depends on the spectrum of the emission being considered. For the band-averaged data, we simply adopt the values 23, 33, 41, 61 and 94 GHz for K- through W-band. Finally, we converted the *WMAP* data from thermodynamic temperature to brightness (antenna) temperature units, in order to make the data consistent with the templates.

3.2 Synchrotron templates

Synchrotron emission arises from the acceleration of cosmic ray electrons in the magnetic field of our Galaxy. This is the dominant Galactic emission at frequencies lower than 10 GHz, with an intensity that depends on the Galactic magnetic field, on the energy spectrum of the electrons and on their spatial distribution. The resulting synchrotron emission is generally described by a power-law spectrum

$$T(\nu) \sim \nu^{-(p+3)/2} = \nu^{-\beta_s} \tag{7}$$

² *Legacy Archive for Microwave Background Data Analysis* – <http://lambda.gsfc.nasa.gov/>.

³ <http://healpix.jpl.nasa.gov>.

where the index p is the spectral index of the energy spectrum of the electrons, and the parameter β_s is the synchrotron spectral index. The spectral behaviour changes with the frequency as a consequence of the details of the cosmic ray electron propagation, including energy loss, and degree of confinement.

The 408 MHz radio continuum all-sky map of Haslam et al. (1982) is dominated by synchrotron emission away from the Galactic plane. Some contribution from free-free emission is observed at the lowest latitudes, for example Reich & Reich (1988) estimate the relative fraction at $b = 0^\circ$ to be of order 10–20%. However, the contribution at intermediate and high latitudes is effectively negligible and hence the 408 MHz sky map is generally assumed as the default template for the synchrotron foreground component. Studies indicate a range of spectral indices β_s from 2.3 to 3.0 between 408 MHz and 1420 MHz (Reich & Reich 1988) and the presence of spurious baseline effects in the survey (Davies et al. 1996) that affect the spectral index determination for weaker features. The combination of these effects, plus the large frequency gap between 408 MHz and microwave wavelengths, does suggest that the sky map scaled by a single effective index may not be representative of the synchrotron emission at *WMAP* frequencies. Nevertheless, its use for foreground studies is well established in the CMB literature and we retain it here. However, we also use the difference between the K and Ka *WMAP* data as a synchrotron template, as suggested by Hinshaw et al. (2007). This at least in part compensates for possible errors introduced by using the Haslam template, presumably accounting for the change in morphology of the emission at microwave frequencies. Moreover, using this template with a single fitted scaling per frequency is likely to be sufficiently accurate even given modest departures from a single spectral index. It is also likely to be a good choice because the intrinsic systematic measurement errors are smaller than for the Haslam map. However, the interpretation of the scalings is complicated by the fact that the difference map must also include a free-free component, and probably a contribution from the anomalous dust correlated emission.

3.3 H α free-free template

The free-free emission arises from electron-ion scattering. Its spectrum is generally described by a power law $T_A \sim \nu^{-\beta_{ff}}$ with $\beta_{ff} = 2.15$ at high-frequency ($\nu > 10$ GHz) and $\beta_{ff} = 2$ at low frequency, due to optically thick self-absorption. Because the free-free emission does not dominate the sky intensity at any radio frequency, our knowledge about it come from H α radiation: both are connected to the ionized interstellar medium and proportional to the *Emission Measure* $EM = \int n_e^2 dl$, where n_e is the electron volume density.

Finkbeiner et al. (2003) has produced an all-sky H α -map by assembling data from several surveys: the Wisconsin H–Alpha Mapper (WHAM) (Haffner et al. 2003), the Virginia Tech Spectral-Line Survey (VTSS) (Dennison et al. 1998), and the Southern H-Alpha Sky Survey Atlas (SHASSA) (Gaustad et al. 2001). The final resolution of the map is asserted to be equal to 6 arcmin. At intermediate and lower Galactic latitudes the absorption of the H α emission by dust is significant and this requires correction if the template is to be used as a tracer of the free-free emission. Dickinson et al. (2003) have used the Schlegel et al. (1998) (SFD) dust map derived from the IRAS 100 μm all-sky survey corrected to a fixed temperature of 18.3 K to estimate the absorption correction. Its amplitude in magnitudes at the H α wavelength is equal to $A(\text{H}\alpha) = (0.0462 \pm 0.0035) D^T f_d$, where D^T is the SFD temperature-corrected 100 μm intensity in MJy sr $^{-1}$ and f_d is the fraction of dust in front of the H α in the line of sight. A value of $f_d \sim 0.5$ is expected under the assumption that the ionised gas and dust are uniformly mixed along the line of sight. However, Dickinson et al. (2003) have presented evidence for a lower value $f_d \sim 0.3$, whilst Banday et al. (2003) suggest that zero correction is required for high Galactic latitudes ($|b| > 20^\circ$). This is the value that we have adopted in our analysis.

After correction the brightness temperature T_b can be related to the EM (in units of cm $^{-6}$ pc) using $T_b \propto T_e^{-0.35} \nu^{-2.1} \times EM$. T_e of ionised gas varies as $\nu^{-0.7}$ in the conversion of H α intensity to brightness temperature at microwave frequencies. For the *WMAP* bands K, Ka, Q, V and W this corresponds to 11.4, 5.2, 3.3, 1.4 and 0.6 $\mu\text{K R}^{-1}$ respectively for $T_e = 8000$ K; see Dickinson et al. (2003) for details.

3.4 Dust templates

Thermal dust emission is the dominant foreground component at frequencies in the range $\sim 100 - 1000$ GHz. Its emissivity is generally approximated by a modified black body law

$$I(\nu) \sim \nu^{\alpha_d} B_\nu(T_d) \quad (8)$$

where α_d is the emissivity index and $B_\nu(T_d)$ the blackbody emissivity at a dust temperature T_d . In fact, different type of dust grains (silicates and carbonates) exhibit different spectra characterized by a range of emissivity indices and dust temperatures. Finkbeiner et al. (1999) developed a series of models (FDS) based on the *COBE*-DIRBE 100 and 240 μm maps tied to the *COBE*-FIRAS spectral data in the range 0.14 to 3.0 mm. Model 8 is considered to be the preferred model at microwave wavelengths and comprises two components with spectral indices $\alpha_{d1} = 1.67$ and $\alpha_{d2} = 2.7$ and temperatures 9.4 K and 16.2 K respectively. Over the *WMAP* range of frequencies, the thermal dust emission in antenna temperature is sometimes considered to scale with a power-law dependence $T_A \sim \nu^{\beta_d}$, with values of 1.7 – 2.2 for β_d assumed by different authors. We

adopt the FDS8 predicted emission at 94 GHz as the reference template for dust emission and compute a single global scaling between this template and the *WMAP* frequencies. The map has a claimed nominal resolution of 6.1 arcmin.

At frequencies between ~ 10 and 100 GHz considerable evidence has been accrued for a foreground component with a synchrotron-like spectrum that is at least partially spatially correlated with the thermal dust emission (Kogut et al. 1996a,b; Banday et al. 2003; Maino et al. 2003; Leitch et al. 1997; de Oliveira-Costa et al. 1998a; Bennett et al. 2003; Hinshaw et al. 2007; Finkbeiner et al. 2002; Casassus et al. 2004). Several models have been advanced to explain the origin of the so-called anomalous dust emission, although a definitive model remains unclear. The *WMAP* science team prefer an interpretation in which the emission is flat-spectrum synchrotron emission that originates in star-forming regions close to the plane. The more commonly accepted theoretical model is that the emission arises from spinning dust grains, ie. the rotational modes of excitation of very small dust grains with a high rotation velocity (Draine et al. 1998a,b). We clearly need an accurate template for this anomalous emission to model the foreground amplitudes at *WMAP* frequencies, but this remains elusive. Finkbeiner et al. (2004) and Davies et al. (2006) have proposed that the FDS template modulated by some power-law of the dust temperature provides a better fit than the unperturbed sky map. However, Bonaldi et al. (2007) suggest that although the anomalous emission is tightly correlated with thermal dust, the correlation is not perfect. Nevertheless, we expect that the FDS model will provide a representative template for our analysis.

4 MONTE CARLO SIMULATIONS AND CALIBRATION OF METHOD

As the first step of our analysis, we have tested FASTICA using realistic simulations of the *WMAP* observations to calibrate the accuracy of the method for template fitting. Specifically, we performed 1000 simulations of the microwave sky at each of the 5 *WMAP* frequencies, each containing a realisation of the CMB signal, the Galactic foreground emission, and instrumental noise appropriate to the specific channel. The study was undertaken at an effective resolution of 1° .

Each simulation was used as an input to FASTICA, together with the foreground emission templates, and the scaling factors computed. Appendix A provides full details of their statistical distribution as a function of both the applied Galactic cut ($Kp2$ or $Kp0$), and the FASTICA non-linear function. In summary, the main conclusions are as follows:

- the t -function is inappropriate for template fitting – the statistical distributions of the returned coupling coefficients are asymmetric and highly biased with respect to the input values
- the p - and g - functions provide similar results – the distributions of the coupling coefficients are well-described by Gaussians with a weak bias of the mean that is essentially insignificant for our studies.
- there is evidence of cross-talk, specifically an anti-correlation, between the synchrotron and dust coefficients when either the Haslam or K-Ka templates are used to characterise the synchrotron emission. In the latter case, correlation between the template and free-free emission is also seen.
- the results from the simple χ^2 analysis indicate that the uncertainties are significantly larger than for the FASTICA method, substantially so when compared to the p -function. Moreover, the method seems to demonstrate more cross-talk between components than seen for the FASTICA analysis.

The uncertainties for the scaling factors presented in later sections of the paper are derived directly from these simulations.

5 ANALYSIS WITH THE HASLAM MAP AS SYNCHROTRON TEMPLATE.

For our initial analysis we consider template fits to the *WMAP* data for all five frequency bands using FASTICA and the Haslam map as the model for the synchrotron emission. Table 1 summarises the results determined using both p - and g -functions for the $Kp2$ and $Kp0$ sky coverages. The corresponding $Kp2$ results based on a simple χ^2 analysis (see Appendix A for details) are also shown, together with the template fit coefficients used by *WMAP* for their first year foreground correction (Bennett et al. 2003). We can make the following general observations based on these results.

The frequency dependence of the coefficients follows the generally expected trends, and in particular, the synchrotron and free-free coefficients decrease with increasing frequency. The situation with dust emission is more complex: the dust emission decreases from 94 GHz to 61 GHz as would be expected for thermal dust emission. However, there is a strongly increasing contribution from a dust correlated component with decreasing frequency below 61 GHz. This presumably constitutes further evidence for a new emission mechanism for dust, the precise physical nature of which remains unknown. Overall, however, there is a minimum contribution from the diffuse Galactic foregrounds at ~ 61 GHz, which can be regarded as defining the optimal range for CMB temperature measurements.

The amplitude of the derived coefficients depends on the extent of the mask applied to the data. For all the foreground components, almost without exception, the coefficients derived with the $Kp0$ sky coverage are less than for $Kp2$. This systematic trend presumably results from genuine spectral variations of the foregrounds on the sky. Indeed, this behaviour is particularly noticeable for the free-free emission, and may reflect the fact that the $Kp0$ mask excludes strong emission regions

	synchrotron		dust		free-free	
	$Kp2$	$Kp0$	$Kp2$	$Kp0$	$Kp2$	$Kp0$
FASTICA - function p						
K	6.64 ± 0.44	5.46 ± 0.62	5.77 ± 0.26	4.94 ± 0.33	8.58 ± 0.39	6.70 ± 0.63
Ka	2.00 ± 0.43	1.68 ± 0.61	2.02 ± 0.26	1.28 ± 0.32	4.31 ± 0.38	2.68 ± 0.62
Q	1.01 ± 0.42	0.87 ± 0.60	1.08 ± 0.26	0.42 ± 0.31	2.89 ± 0.38	1.36 ± 0.61
V	0.26 ± 0.40	0.26 ± 0.55	0.60 ± 0.24	0.03 ± 0.28	1.39 ± 0.36	0.01 ± 0.57
W	0.05 ± 0.35	0.05 ± 0.49	0.95 ± 0.21	0.46 ± 0.25	0.67 ± 0.32	-0.49 ± 0.52
FASTICA - function g						
K	6.52 ± 0.54	5.66 ± 0.80	6.07 ± 0.29	5.71 ± 0.41	8.52 ± 0.54	6.60 ± 0.82
Ka	2.05 ± 0.53	1.87 ± 0.79	2.09 ± 0.28	1.66 ± 0.40	4.21 ± 0.53	2.75 ± 0.80
Q	1.09 ± 0.52	1.08 ± 0.78	1.11 ± 0.28	0.69 ± 0.40	2.79 ± 0.53	1.47 ± 0.79
V	0.39 ± 0.49	0.56 ± 0.72	0.58 ± 0.27	0.19 ± 0.36	1.31 ± 0.50	0.19 ± 0.76
W	0.18 ± 0.43	0.31 ± 0.65	0.93 ± 0.23	0.59 ± 0.32	0.61 ± 0.43	-0.36 ± 0.67
χ^2 analysis						
K	5.96 ± 0.57		6.38 ± 0.29		8.00 ± 0.62	
Ka	1.83 ± 0.56		2.25 ± 0.29		3.71 ± 0.60	
Q	0.94 ± 0.54		1.24 ± 0.28		2.32 ± 0.58	
V	0.18 ± 0.49		0.69 ± 0.25		0.88 ± 0.53	
W	0.01 ± 0.37		1.02 ± 0.19		0.23 ± 0.41	
Bennett et al. values (constrained: $\beta_s = 2.7$; $\beta_{ff} = 2.15$)						
K	–		–		–	
Ka	–		–		–	
Q	1.01		1.04		(1.92)	
V	0.34		0.62		(0.82)	
W	0.11		0.87		(0.32)	

Table 1. Values of the coupling coefficients in antenna temperature units determined between the 3-year WMAP data and three foreground emission templates, at 1° resolution. The Haslam 408 MHz map is adopted as the synchrotron template. The FASTICA analysis is performed using the two non-linear functions p and g and for the $Kp2$ and $Kp0$ masks. The corresponding $Kp2$ results for a simple χ^2 analysis are provided for comparison. In addition, we provide the values from the Bennett et al. (2003) fits to the Q , V and W -bands performed with constraints imposed on the synchrotron and free-free spectral indices. These are the coefficients adopted by WMAP for their first-year foreground corrections. The units are $\mu K/K$ for synchrotron, mK/mK for dust and $\mu K/R$ for free-free emission respectively.

near the Galactic plane, whilst the free-free emission remains weak at higher latitudes. These strong emission regions may also manifest real variations in scaling dependence relative to the $H\alpha$ template due to variations in the dust absorption or in the temperature of the ionised gas in the medium latitude region present in the $Kp2$ mask but removed by $Kp0$.

The FASTICA numbers are also in good statistical agreement with our own simple χ^2 results, provided only for the $Kp2$ sky coverage. Interestingly, the synchrotron and dust amplitudes are systematically lower (higher) for the χ^2 method. However, these results in general reflect the weak cross-talk seen between the fitted amplitudes in Appendix A. The free-free amplitudes are also typically $1\text{-}\sigma$ higher for the FASTICA analysis.

Similarly, the constrained fits from Bennett et al. (2003) are of comparable amplitude for the synchrotron and dust coefficients. These values were derived by fixing the synchrotron spectral index at a value of 2.7, and the free-free to 2.15 for frequencies above Q-band. The former constraint explains why the synchrotron amplitude remains higher at V- and W-band for the first-year WMAP corrections, although the Q-band amplitude is in excellent agreement with the FASTICA numbers. It is curious to note that the constrained synchrotron index adopted is inconsistent with the Q-band amplitude, from which one can infer a spectral index of ~ 3 between 408 MHz and 61 GHz. However, Bennett et al. (2003) specifically state that their template method is not particularly physical, but removes foregrounds outside the $Kp2$ cut at the required level.

Finally, we would like to comment on the impact of dipole subtraction for the analysis. Specifically, the results we have presented here, including those of Bennett et al. (2003), do not subtract a best-fit dipole amplitude from the data and templates before fitting the template amplitudes. Since other independent analyses, eg. Davies et al. (2006), do prefer to remove the dipole, we have tested its impact on the results. In fact, we find that the dust and free-free coefficients remain largely unchanged, whilst the synchrotron values become negative at high frequencies. It may be that this is connected with the projection of the North Polar Spur in the Haslam template onto the best-fit dipole computed for that template.

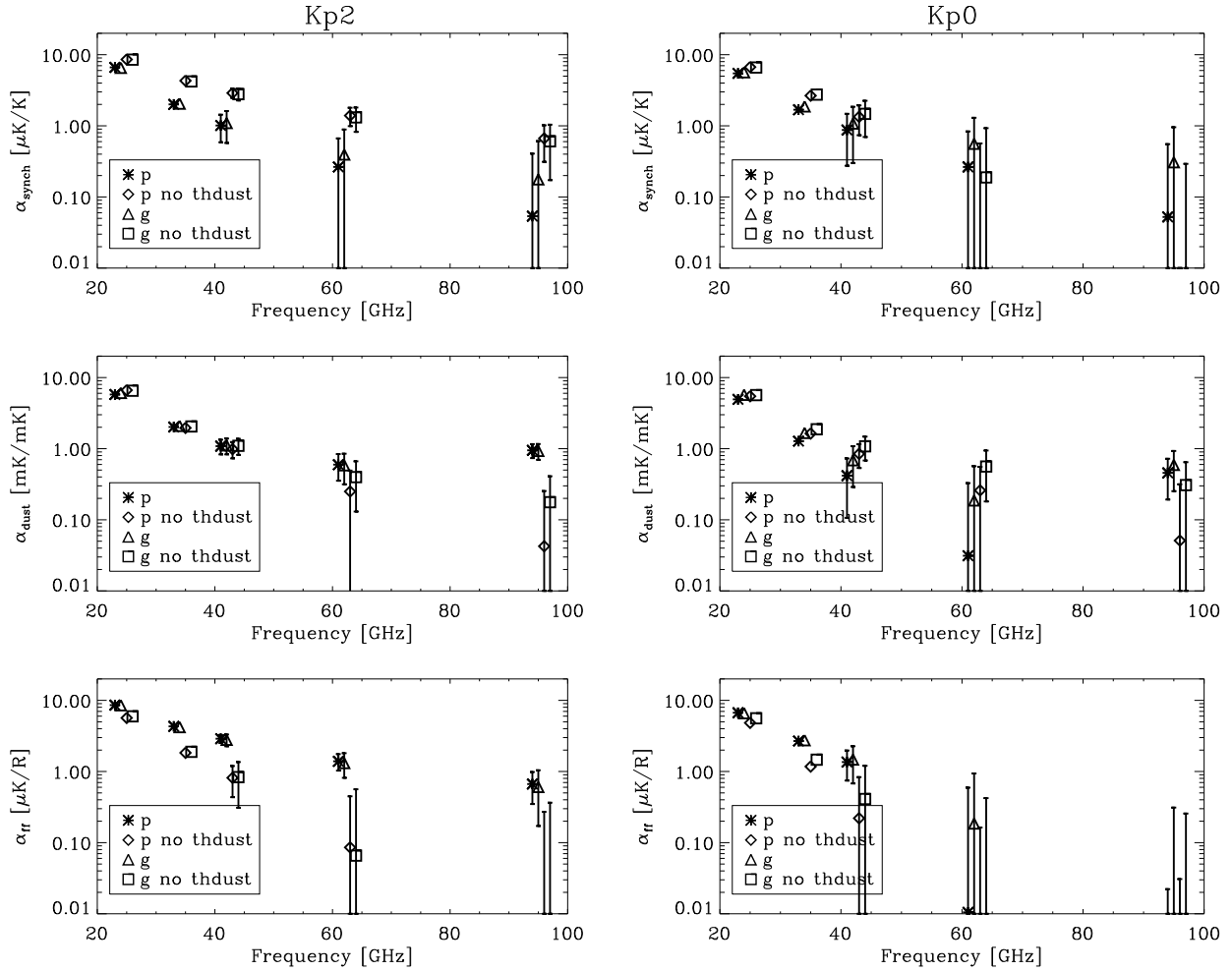


Figure 1. Comparison between scaling factors obtained from *WMAP* data with and without the thermal dust emission, at the resolution of 1° . At the lowest frequencies, the error bars are smaller or comparable to the size of the plot symbols. The only significant change is at *W*-band for the dust coefficients.

5.1 Spectral index of foreground emissions.

We utilise the derived frequency dependence of the scaling factors to parameterise the spectral behavior of the foreground emission components. For each component, we fit the corresponding coefficients with a power law model of the form $A_{norm}(\nu/\nu_0)^{-\beta}$. A_{norm} is the amplitude of the emission of a specific physical component at the reference frequency ν_0 , which we take as the *K*-band (23 GHz).

The results for the synchrotron emission generally indicate a steep spectral index consistent with a value in excess of $\beta_s = 3.0$. Curiously, the index is flatter for the *Kp0* mask, particularly when using the *g*-function. The amplitudes, however, fall with decreasing sky coverage – this is generally true for all of the emission components, suggesting that there remains within the *Kp2* to *Kp0* transition region emission that differs in nature from genuine high latitude emission. It is also interesting to note that the amplitude at 23 GHz implies a spectral index of ~ 3 relative to the 408 MHz emission, so that in general there are hints of steepening at higher frequencies, as has been previously noted by the *WMAP* team.

Since the *WMAP* frequency range does not allow a detailed study of the spectral behaviour of the thermal dust component, we consider the spectral properties of the anomalous dust correlated emission. Understanding the nature of this component remains of great importance for the study of CMB anisotropy and for motivating physical models of the emission. We use a single dust template to specify the morphology of both the thermal dust emission and the anomalous dust correlated component. Thus, in order to study the latter cleanly, we must apply a correction for the thermal dust contribution. Specifically, the scaling factors have been recomputed using *FASTICA* after subtracting the dust template from the data assuming that the *FDS8* dust model (see section 3.4) provides an exact model of this emission component. Under this assumption a persistent correlation with the dust template will be due to the anomalous component, spatially correlated with the thermal dust, but with a different physical nature. Figure 1 shows the scaling factors for the dust emission without the thermal

	Synchrotron		Anomalous Component		Free-Free	
	<i>Kp2</i>	<i>Kp0</i>	<i>Kp2</i>	<i>Kp0</i>	<i>Kp2</i>	<i>Kp0</i>
FASTICA – function p						
β	3.35 ± 0.47	3.28 ± 0.79	3.29 ± 0.32	4.48 ± 0.78	1.87 ± 0.15	2.92 ± 0.55
A_{norm}	6.64 ± 0.43	5.46 ± 0.62	5.68 ± 0.26	4.85 ± 0.33	8.56 ± 0.38	6.79 ± 0.63
FASTICA – function g						
β	3.10 ± 0.53	2.82 ± 0.80	3.35 ± 0.35	4.14 ± 0.75	1.92 ± 0.22	2.72 ± 0.65
A_{norm}	6.51 ± 0.53	5.62 ± 0.80	5.98 ± 0.29	5.63 ± 0.41	8.51 ± 0.52	6.68 ± 0.81

Table 2. Spectral index β and normalisation factor A_{norm} obtained fitting values of the coupling coefficients for synchrotron, the anomalous component of dust and free-free emission, with different masks.

component, compared with the values of the original analysis. In fact, the values differ significantly for the dust coefficients only at 61 and 94 GHz as might be expected since the thermal component falls off rapidly with decreasing frequency. Note also that whatever dust residuals remain at the highest frequency are statistically insignificant, providing strong support to the FDS8 model of thermal dust emission.

The values of the spectral index β_a of the anomalous dust component determined on the *Kp2* sky coverage are somewhat steeper than the value of 2.85 obtained by Davies et al. (2006). However, they have also noted spectral indices as steep as 3.8 in several dust dominated regions at mid- to high-latitude. As with the synchrotron component, the amplitude of the emission drops for the *Kp0* mask, and consequently the spectral index steepens noticeably. One might speculate that this is related to the differing properties of the anomalous component closer to the Galactic plane flattening the index of the *Kp2* results. In the context of the spinning dust models proposed by Draine et al. (1998a) to explain the anomalous emission, the behaviour may reflect the properties of the spinning dust in different phases of the interstellar medium, eg. a greater or lesser admixture of spinning dust in the warm ionised medium (WIM) depending on latitude.

Finally, we consider the properties of the free-free emission as represented by the coupling coefficients determined relative to the $H\alpha$ template. Indeed, before determining the specific spectral behaviour, it is worth noting that the derived coefficients are not in accord with expectations for the $H\alpha$ to free-free conversion factor for which a value of 8000 K is conventionally adopted for the thermal electron temperature. In fact, the K- and Ka-band results for *Kp2* sky coverage are more consistent with temperatures in the range 5000-6000 K. Curiously, however, the coefficients at higher frequencies are increasingly consistent with a higher temperature value. In terms of a power-law fit for the frequency spectrum, this corresponds to a notably flatter spectral index than the typical value of 2.14 for free-free emission, with the best-fit value for the *p* function FASTICA fits some 2σ away from this canonical amplitude. However, the results when a *Kp0* mask is applied are significantly different, favouring an even steeper slope than expected for free-free, and with normalisation amplitudes corresponding to an electron temperature below 4000 K. This latter behaviour was also observed by Davies et al. (2006) for 5 regions specifically selected to be dominated by free-free emission.

In order to assess the consistency of our results with the theoretically motivated spectral index as compared to the apparently anomalous best-fit models, we have fitted the values of the coupling coefficients by an idealised model for the free-free emission, $A_{norm}(\nu/\nu_0)^{-2.14}$, and evaluated the goodness-of-fit of the model. The results are consistent with the $\beta_{ff} = 2.14$ model, even in the case of the *Kp0* mask. However, in a set of 1000 simulations in which the simulated free-free emission followed the theoretically motivated spectrum, no cases were found for which there were such large changes in the fitted spectral slopes determined for *Kp2* or *Kp0* sky coverage as those observed with the data. This could reflect the ideal nature of the simulated emission, but irrespective of this, although our results are statistically consistent with the expected free-free scaling with frequency, there are inconsistencies that are difficult to reconcile.

Arguably then, the FASTICA result for the *Kp2* mask could be considered an independent verification of the behaviour observed in Dobler et al. (2008a). Motivated by their analysis, we augment our assessment of the free-free spectral behaviour by fitting the coefficients in intensity units. The results are presented in Table 3 and Figure 2. Dobler et al. (2008a) found that the $H\alpha$ -correlated emission showed a bump near to 50 GHz, although the exact behaviour was sensitive to the type of CMB estimator that they pre-subtract from the WMAP data before fitting template amplitudes. In our analysis, no such subtraction is necessary, since the coefficients are essentially determined as part of the process of deriving the best CMB estimate from the data. In fact, our *Kp2* amplitudes show more extreme behaviour at high frequencies, and indicate a systematically rising spectrum, although the best-fit is also consistent within errors with the slowly falling theoretically expected spectrum. However, our *Kp0* results are significantly steeper than either the *Kp2* or expected slopes. Referring again to the results from the regional analysis of Davies et al. (2006), there is a wide range of spectral behaviour, with region 1 exhibiting a steeper rise in frequency than seen here for *Kp2*, region 5 being somewhat consistent with the observations

Free-Free - Intensity				
	FASTICA – function p		FASTICA – function g	
	<i>Kp2</i>	<i>Kp0</i>	<i>Kp2</i>	<i>Kp0</i>
β	0.13 ± 0.15	-0.92 ± 0.55	0.08 ± 0.22	-0.72 ± 0.65
A_{norm}	0.14 ± 0.01	0.11 ± 0.01	0.14 ± 0.01	0.11 ± 0.01

Table 3. Spectral index β and normalisation factor A_{norm} obtained fitting values of the intensity coupling coefficients for free-free emission, with different masks.

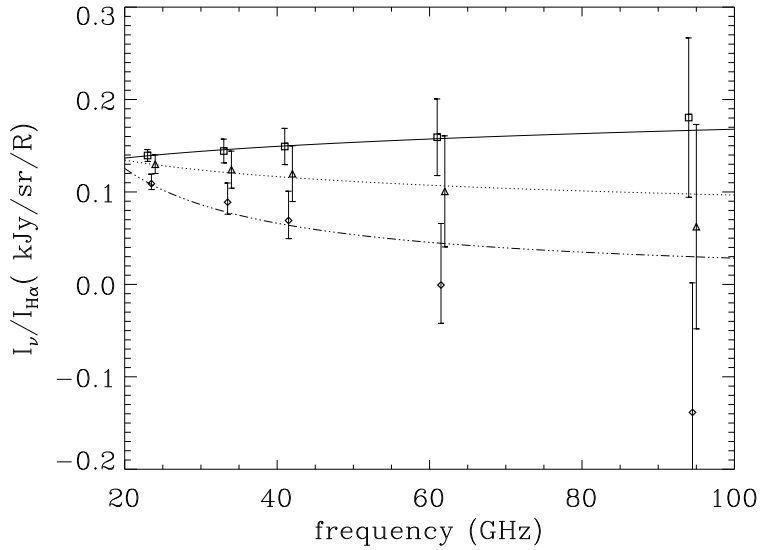


Figure 2. The coupling coefficients in intensity units for free-free emission as traced by the $H\alpha$ template. Squares represent the derived amplitudes for *Kp2* sky coverage from the FASTICA *p*-function analysis, diamonds are for the corresponding analysis on *Kp0*, whilst triangles show the results for a simple χ^2 analysis on *Kp2*. Best-fit curves are also shown. The FASTICA *Kp2* results show an anomalous rising spectrum for the free-free emissivity, whereas the *Kp0* and χ^2 *Kp2* are steeper than expected, the former significantly so.

here, but most regions falling off rapidly. Interestingly, the simple χ^2 analysis, for which a best-fit spectral index of 0.2 ± 0.3 is found, is very consistent with theoretical expectations (~ 0.14).

The major difference between all of these results is how the method treats the CMB contribution. Dobler et al. (2008a) subtract an estimate of the CMB based on a variant of the *WMAP* ILC method, Davies et al. (2006) explicitly include a CMB covariance term in fitting the data directly with three templates, our χ^2 analysis simply ignores the CMB contribution in fitting the templates, whilst the FASTICA method is specifically attempting to construct the best estimate of the CMB sky and computing template coefficients accordingly. Clearly more work is needed to understand the relative merits and problems in these approaches.

Finally, Dobler et al. (2008b) interpret the results of both their full-sky analysis and an assessment of the Gum nebula region in terms of an enhanced emissivity due to a spinning dust contribution from the WIM. It is difficult to make a statement either in support or against this conclusion based on our results, given the large difference between the fits on *Kp2* and *Kp0*, and the apparent dependence on the CMB subtraction method. Perhaps it reflects the different properties of the free-free emission close to the plane, or the presence indeed of spinning dust in the WIM, or simply cross-talk between different physical components that confuses the spectral analysis. However, we remind the reader that our fits for both *Kp2* and *Kp0* sky coverage are statistically consistent with the expected scaling for free-free emission with frequency, $\beta_{ff} = 2.14$.

5.2 Single Year Analysis

In order to test the stability of the coupling coefficients between the foreground templates and the *WMAP* data to potential systematics, eg. annual instrumental or calibration variations, we have performed the same FASTICA analysis for the yearly

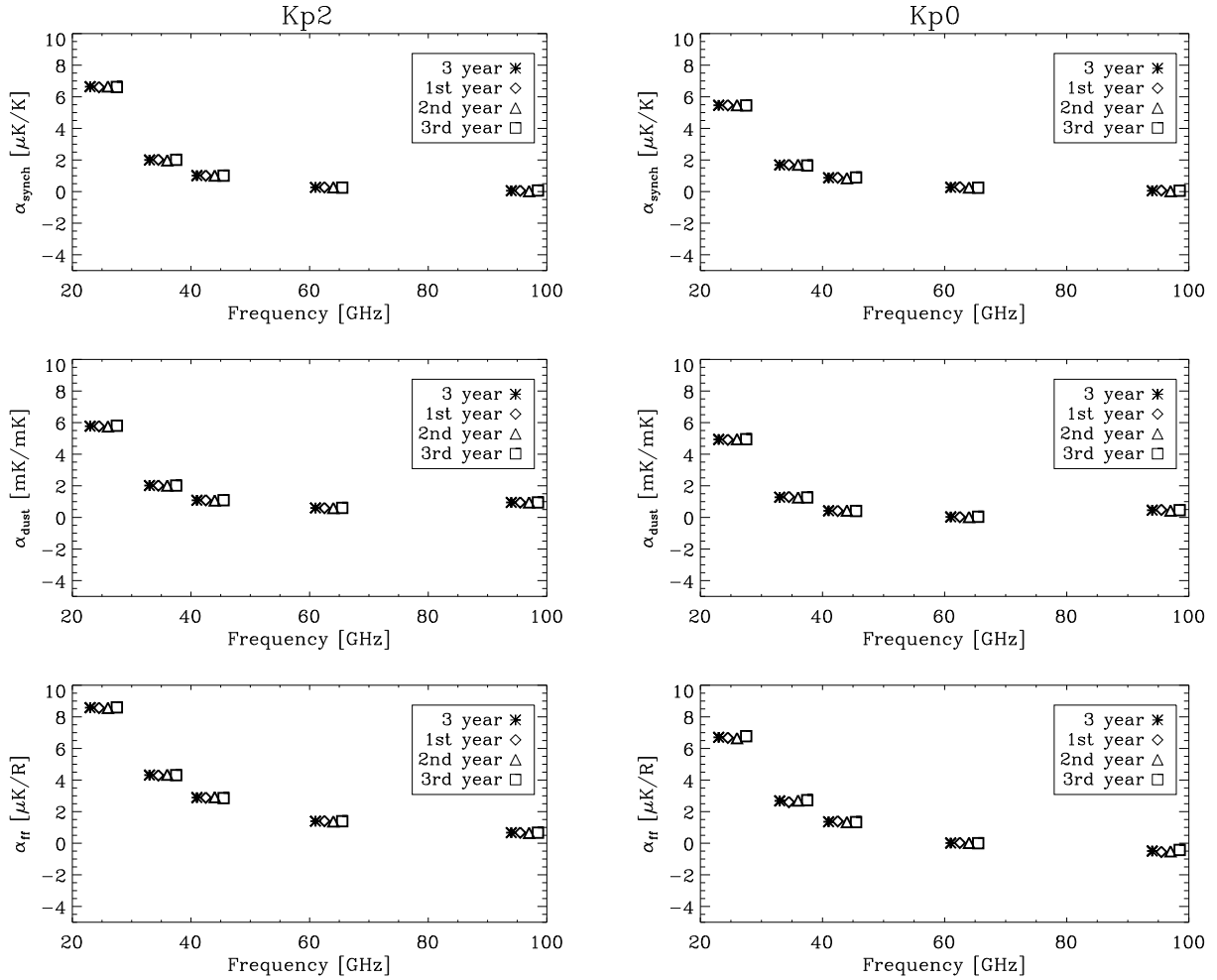


Figure 3. Comparison between scaling factors determined for the yearly WMAP sky maps. The results for the 3-year WMAP data are also shown for reference. All results are determined using the FASTICA p -function.

sky maps. These results are plotted in Figure 3 together with the 3-year data coefficients. We find no evidence of significant annual variations in the coefficients.

6 ANALYSIS WITH THE K-KA MAP AS SYNCHROTRON TEMPLATE.

One of the limitations of the previous foreground analysis is that the Haslam map used as template for the synchrotron emission is unlikely to be completely representative of the foreground morphology at the WMAP frequencies due to spectral index variations across the sky. Therefore, we repeated the analysis using the K-Ka map as an internal template for the synchrotron emission. We then computed the scaling factors for the Q, V and W channels. The results are shown in Table 4. As before, the uncertainties of the coupling coefficients have been computed from 1000 simulations. Once again, the p -function seem to be statistically more robust than the corresponding g -function ones.

Table 4 also contains results returned by the χ^2 minimisation method, both our own and those from WMAP (Hinshaw et al. 2007). For our analysis, we did not impose any constraints on the spectral behaviour of the various physical components. In contrast, Hinshaw et al. (2007) explicitly account for the free-free ($\beta_{ff} = 2.14$) and thermal dust ($\beta_d = 2$) spectral indices. The coefficients derived for the K-Ka and dust templates are in excellent agreement for all three methods. The free-free values, however, are notably different in all three cases. The difference to the WMAP results could, at least in part, be due to their application of a large correction for dust absorption, although comparing coefficients at all three frequencies the explanation is clearly more complex. A more useful observation in regard to the free-free coefficients is that they are universally lower than in the corresponding Haslam case for the Q-band but almost identical for W-band. This directly reflects the fact that the K-Ka template contains not only

	Synchrotron		Dust		Free-free	
	<i>Kp2</i>	<i>Kp0</i>	<i>Kp2</i>	<i>Kp0</i>	<i>Kp2</i>	<i>Kp0</i>
FASTICA - function p						
<i>Q</i>	0.24 ± 0.04	0.21 ± 0.07	0.17 ± 0.32	-0.13 ± 0.41	1.92 ± 0.42	0.48 ± 0.70
<i>V</i>	0.05 ± 0.04	0.03 ± 0.06	0.50 ± 0.29	0.40 ± 0.30	1.19 ± 0.40	-0.16 ± 0.66
<i>W</i>	-0.01 ± 0.03	-0.04 ± 0.05	1.00 ± 0.26	0.77 ± 0.34	0.73 ± 0.35	-0.41 ± 0.58
FASTICA - function g						
<i>Q</i>	0.24 ± 0.09	0.16 ± 0.15	0.16 ± 0.52	0.03 ± 0.80	1.76 ± 0.66	0.84 ± 0.98
<i>V</i>	0.06 ± 0.08	-0.004 ± 0.14	0.23 ± 0.76	0.39 ± 0.50	1.05 ± 0.63	0.16 ± 0.93
<i>W</i>	0.01 ± 0.072	-0.05 ± 0.12	0.94 ± 0.44	0.80 ± 0.66	0.56 ± 0.54	-0.20 ± 0.81
χ^2 analysis (no constraints)						
<i>Q</i>	0.21 ± 0.09		0.42 ± 0.50		1.44 ± 0.77	
<i>V</i>	0.03 ± 0.08		0.57 ± 0.46		0.75 ± 0.70	
<i>W</i>	-0.01 ± 0.06		1.10 ± 0.36		0.29 ± 0.54	
Hinshaw et al.						
<i>Q</i>	0.23		0.19		0.99	
<i>V</i>	0.05		0.41		0.63	
<i>W</i>	0.00		0.98		0.32	

Table 4. Values of coupling coefficients in antenna temperature units between the 3-year WMAP *Q*, *V*, and *W*-band data and three foreground emission templates at 1° resolution. The K-Ka map is adopted as the synchrotron template. The FASTICA analysis is performed using the two non-linear functions *p* and *g* and for the *Kp2* and *Kp0* masks. The corresponding *Kp2* results for a simple χ^2 analysis are provided for comparison. In addition, we provide the band-averaged values from the Hinshaw et al. (2007) fits performed with constraints imposed on the free-free and thermal dust spectral indices. Note that the WMAP team used an $H\alpha$ template corrected for dust absorption assuming $f_d = 0.5$ for their analysis. The units are mK/mK for synchrotron, mK/mK for dust and $\mu K/R$ for free-free emission respectively.

synchrotron but also free-free emission. The latter also indicates that the FASTICA results continue to prefer a flatter slope for the free-free emission than expected from theory, and as derived by the χ^2 analysis.

The most interesting results are related to the amplitudes of the coupling coefficients for the dust. In particular, note the low value of the dust contamination in the Q-band in contrast with previous findings for the Haslam case. This could be interpreted as indicating the absence of an anomalous dust correlated component, in apparent contradiction to previous results. However, it is also consistent with a picture in which the K-Ka template contains contributions not only from the synchrotron and free-free emission, but also the anomalous component, which the Haslam map certainly does not. At W-band and for the *Kp2* sky coverage, the K-Ka contribution is essentially zero, so that there is no effective contribution of this embedded anomalous component, and the dust coefficients should be consistent with the thermal dust emission. Indeed, there is again strong support for the FDS model of the thermal dust emission, although for the *Kp0* cut the amplitude drops as before.

In order to understand whether there is a self-consistent picture with the Haslam results, we can perform some simple numerical comparisons. If we assume that the WMAP data contains foregrounds comprised of synchrotron, free-free and anomalous dust contributions as described in Table 1, then we can infer the extent of these components present in the K-Ka template, and then predict the amplitudes expected for the free-free and dust contributions in Table 4 allowing for that fraction contained in the K-Ka map. The consistency is excellent for both *p* and *g* function results on the *Kp2* sky cut, and certainly good for the *Kp0* coverage. We have also made a more detailed study using simulations, with the same results. Of course, this does not imply that the K-Ka template is not a significant improvement on the Haslam map, but that the gross features of the two foreground models are in agreement. The quality of the two synchrotron templates will be considered further in the following sections.

6.1 Spectral properties of foreground emissions.

A study of the spectral index of the returned K-Ka coefficients would be unphysical, or at least difficult to interpret, since the template is a mix of synchrotron, free-free and anomalous dust emission. Moreover, the interpretation of the spectral behaviour of the returned dust and free-free coefficients is similarly problematic, requiring a detailed understanding of the fraction of the signal associated with the K-Ka template. However, it is worth reiterating, as shown above, that the template

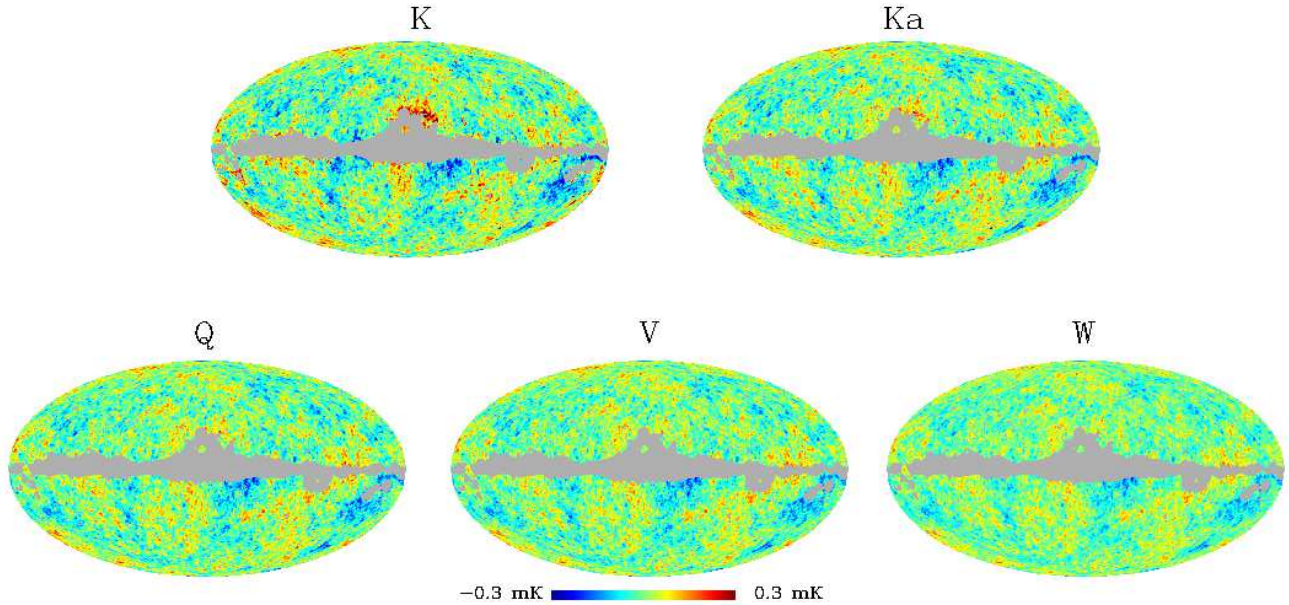


Figure 4. WMAP data for K-, Ka-, Q-, V- and W-bands cleaned by subtracting foreground templates scaled by the coupling coefficients determined by FASTICA with the p -function for the Kp2 sky coverage. Here, the synchrotron template is the Haslam map. The maps are shown in a conventional mollweide projection in a Galactic frame-of-reference, with the north pole at the top of the image and the Galactic Center in the middle with longitude increasing to the left. The regions in grey correspond to the bright Galactic emission and point sources excised from the analysis by the Kp2 mask.

fits are in excellent agreement with those in which the Haslam map is used as the synchrotron template, and therefore the spectral behaviour of the components can be interpreted in the same manner.

7 EVALUATION OF THE Q-, V- AND W-BAND SKY MAPS AFTER FOREGROUND CLEANING

One of the main aims of the foreground analysis performed thus far with FASTICA is to promote the possibility of cleaning the WMAP data sufficiently to allow its use for cosmological purposes. Therefore, adopting the coupling coefficients derived for various foreground templates, we have studied WMAP sky maps cleaned of the Galactic emission.

Figure 4 shows the residual sky signal of the five WMAP channels that have been cleaned using the Haslam data as the synchrotron template. We show only the results based on the p -function analysis, since there is little visual difference relative to the g -function. There are clearly residuals close to the Galactic plane for the K and Ka sky maps, particularly near the edge of the Kp2 mask in the vicinity of the Galactic Centre. This excess foreground emission falls off rapidly with frequency, and only a hint can be seen in the Q-band data. Nevertheless, the dominant frequency-independent CMB structure is clear at high latitudes. Figure 5 shows the equivalent results for the Q-, V- and W-bands when the K-Ka synchrotron template is adopted. There is little visual evidence of residual foregrounds even close to the masked regions.

As an interesting comparison, we have investigated the difference between the cleaned maps obtained using either the Haslam or the K-Ka synchrotron templates, scaled by the coupling coefficients determined either by our FASTICA analysis or by the WMAP team. Figure 6 shows the results for the Q-, V- and W-bands (in neither the first nor second data release did WMAP provide cleaned K- or Ka-data, presumably because they do not utilise them for cosmological analysis). The main difference apparent at Q-band is the presence of a bright structure around the mask concentrated near the Galactic Centre both above and below the plane. This is a clear delineation of the K-band residual noted above when using the Haslam template, and is most easily interpreted as Galactic emission that is not traced by the Haslam synchrotron template. It therefore supports the WMAP assertion that adopting the K-Ka map as a template provides a more complete model of the foreground emission at low frequency where other contributions beyond the synchrotron and free-free emission may exist. This structure is seen clearly in both the FASTICA and WMAP residual plots. Also seen is evidence of a negative residual associated with a well-known feature in the low frequency template – the North Polar Spur – plus other residuals around the edge of the Galactic plane part of the Kp2 mask, although whether these are more associated with the Haslam or K-Ka analysis is unclear.

The residuals at V- and W-bands show much fainter features, and particularly for the FASTICA analysis. Indeed, in this

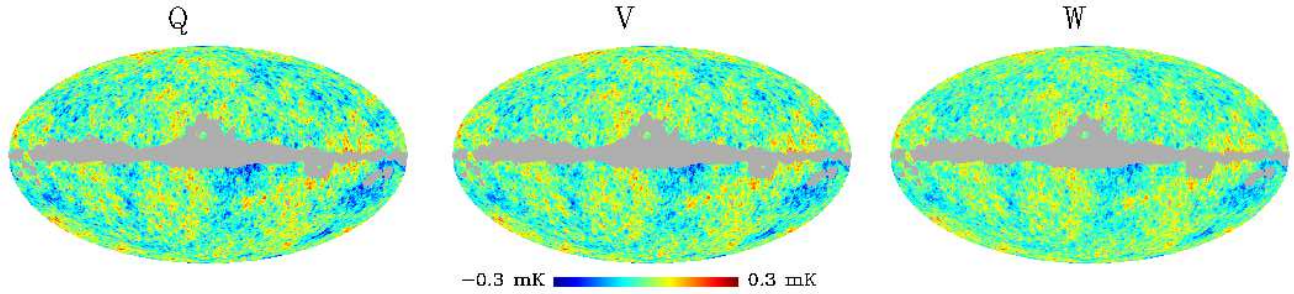


Figure 5. WMAP data for Q-, V- and W-bands cleaned by subtracting foreground templates scaled by the coupling coefficients determined by FASTICA with the p -function. Here, the synchrotron template is the K-Ka map.

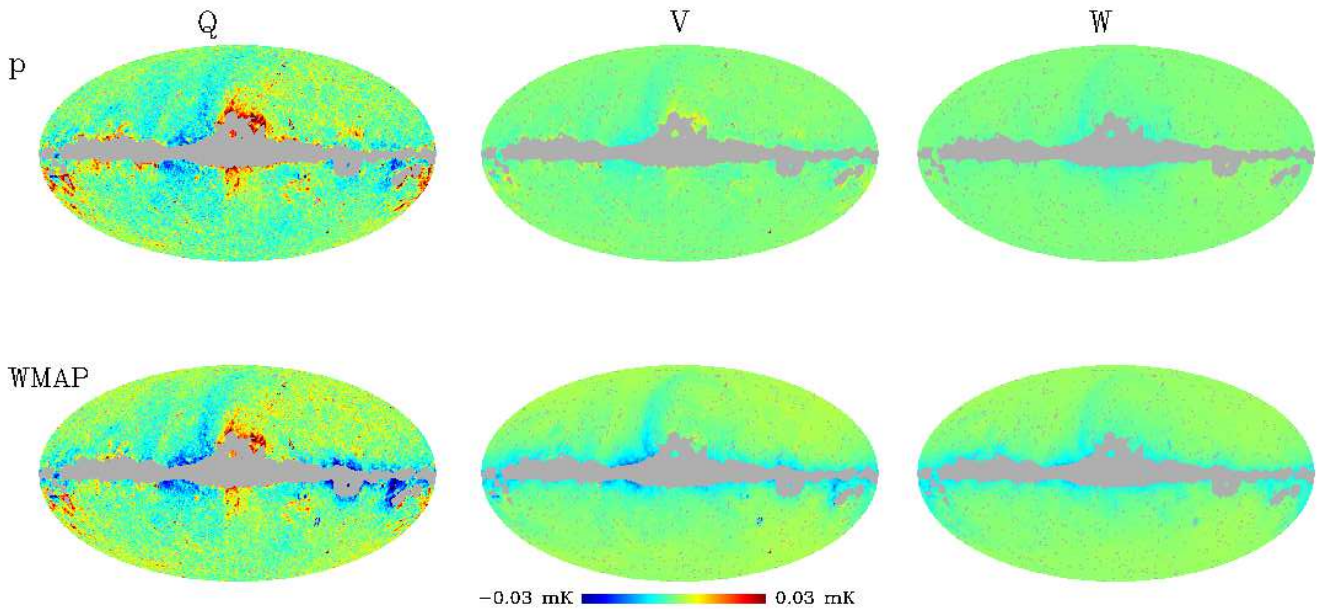


Figure 6. Difference between the cleaned maps using the Haslam map and the K-Ka map at 41, 61 and 94 GHz. The top row shows the difference when the FASTICA p -function coefficients are used, the lower line shows the equivalent difference maps from when applying the WMAP first-year and three-year foregrounds corrections.

case the plot indicates that the total foreground level determined using either the Haslam or K-Ka maps, plus the usual tracers of free-free and dust emission, are in very good agreement. This is consistent with the discussion in the previous section. For the data corrected using the WMAP template coefficients, the residuals seem to be larger in all cases.

The comparison here cannot easily be used to infer whether the FASTICA template fits are to be preferred to the WMAP ones, but we will attempt to address this issue in the next section. What should be clear is that it is always good practise for a cosmological analysis to study the cleaned maps at different frequencies and test for evidence of a frequency dependence that is the signature of foreground residuals.

In fact, we do exactly that by examining the power spectra of the cleaned maps determined using the MASTER algorithm (Hivon et al. 2002). Figure 7 indicates that the maps are essentially insensitive to the residual foreground features that remain in the data due to the different fitting methods and templates, although the quadrupole amplitude is generally suppressed, and notably so when using the Haslam template to trace synchrotron emission. Thus the cleaned maps, particularly at V- and W-bands, can be considered adequate for cosmological analyses, at least when based on the angular power spectrum.

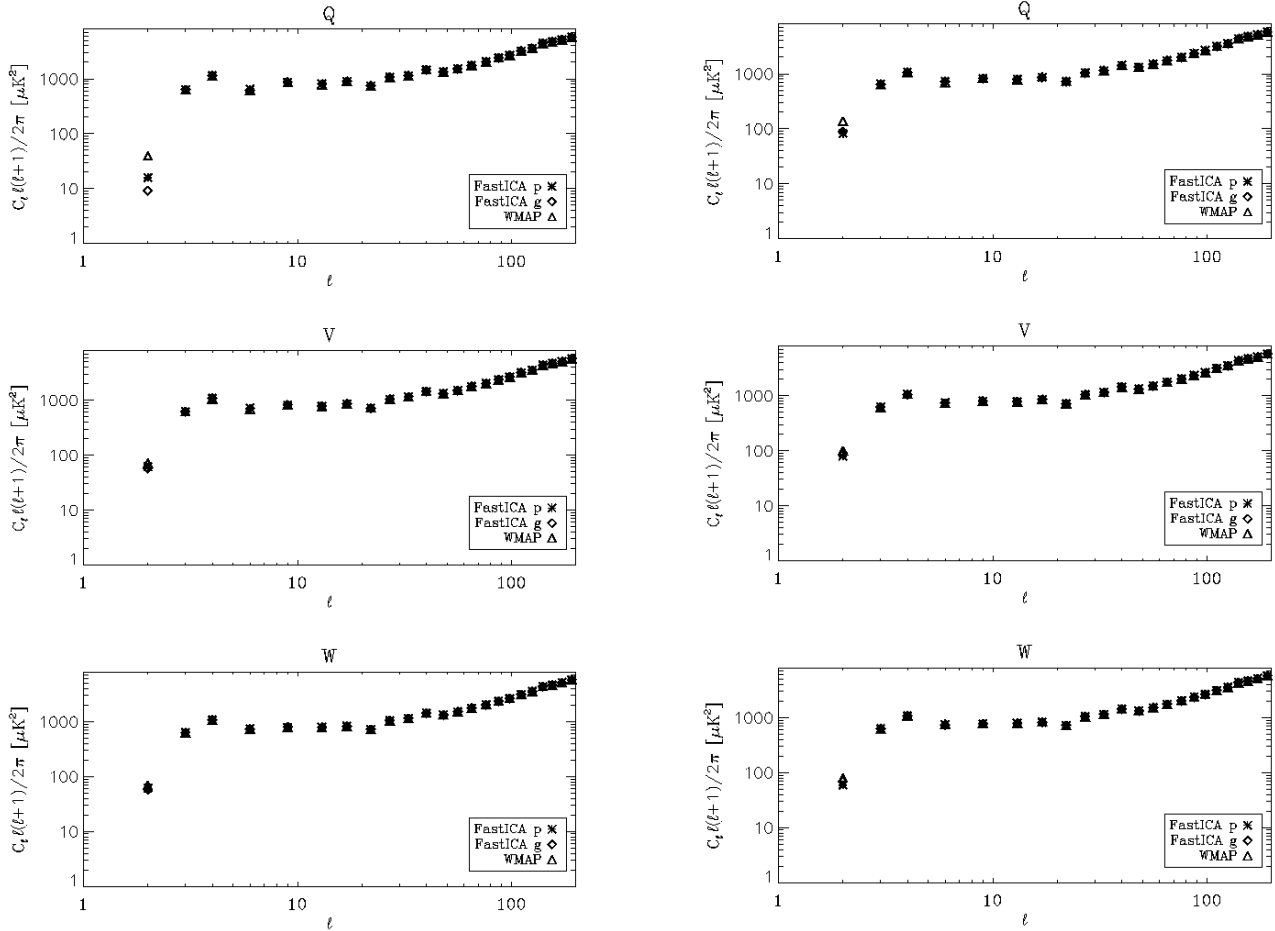


Figure 7. Left: Binned power spectra of the Q-, V- and W-maps cleaned from the foreground emission. Their contamination is described by the coupling coefficients determined by FASTICA with both the p- and g-functions (asterisk and diamond respectively) and by the WMAP analysis (triangle). The left figure corresponds to the case when the Haslam map is used as the synchrotron template, the right figure to the corresponding analysis using K-Ka for the low-frequency emission.

8 AN ‘ITERATIVE’ BLIND COMPONENT SEPARATION STUDY USING WMAP DATA PRE-CLEANED USING TEMPLATES

As demonstrated in the previous section, the WMAP data cleaned by foreground templates still show evidence of contamination due to either the inability of the templates to describe real spectral variations in the foreground emission on the sky, or other emission mechanisms not identified with the standard Galactic components/templates. Inspired by the analysis of Patanchon et al. (2005), we have performed an ‘iterative’ blind analysis on the WMAP data, *after* pre-cleaning with the foreground templates, in order to study the residuals in more detail.

Various combinations of the cleaned WMAP channels are used as input to the FASTICA algorithm. This then returns a number of components equal to the number of the input sky maps. One of these is identified as a CMB map, cleaned as far as possible from any *residual* emission (see section 8.2). Without exception, at most one of the other returned components can be clearly indentified with Galactic residuals, the remainder generally being some combination of anisotropic noise (reflecting the underlying observation pattern of the WMAP satellite) and weak residual dipole emission. Figure 8 shows maps of the candidate foreground residuals for a number of WMAP and template input permutations, as described in the figure caption and discussed in section 8.1

8.1 Foreground residuals

The upper row of Figure 8 shows the output maps from FASTICA that we identify with foreground residuals when using the Haslam template for synchrotron emission.

The leftmost figure presents results from analysing the five WMAP frequency bands after cleaning using the coefficients previously derived in this paper (see Table 1). There are some bright features along the Galactic plane near to the Galactic

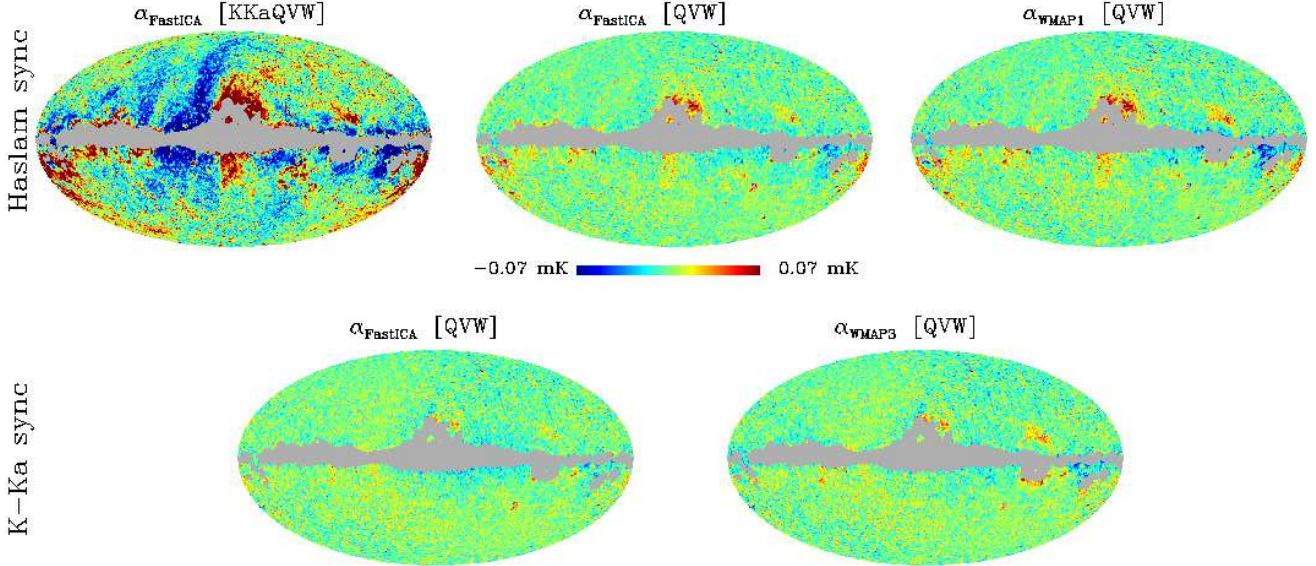


Figure 8. Maps of the residual components obtained by FASTICA when applied to the WMAP data after pre-cleaning using template fits with coupling coefficients α derived either using a FASTICA analysis with the p -function and the Kp2 mask or by the WMAP team in Bennett et al. (2003) (WMAP1) and Hinshaw et al. (2007) (WMAP3). Several cases have been considered: *i*) input maps K-, Ka-, Q-, V- and W-bands plus Haslam synchrotron template, FASTICA coefficients; *ii*) input maps Q-, V- and W-bands plus Haslam synchrotron template, WMAP constrained fit coefficients; *iii*) input maps Q-, V- and W-bands plus K-Ka synchrotron template, FASTICA coefficients; *v*) input maps Q-, V- and W-bands plus K-Ka synchrotron template, WMAP constrained fit coefficients.

Centre and the presence of a structure related to the North Polar Spur. These are a clear indication of the deficiencies of the Haslam map as a synchrotron template, particularly for cleaning the K- and Ka-band data, with which the residuals are predominantly associated. Some of the positive and negative features presumably reflect either under- or over-subtraction of the true foreground signal by the templates as a consequence of spectral variations.

The middle figure shows the equivalent analysis using just the Q-, V- and W-band pre-cleaned sky maps. The residuals are significantly reduced, and no evidence of the North Polar Spur is now observed. The dominant feature, as before, is the structure close to the Galactic centre. This was originally identified and referred to as the ‘free-free haze’ by Finkbeiner et al. (2004) (although its origin as free-free emission is unlikely and it is now referred to as the ‘WMAP haze’), and was already visible in the foreground residuals plot of Bennett et al. (2003). Moreover, the map is strikingly (though perhaps unsurprisingly) similar to the map obtained by Patanchon et al. (2005), using Spectral Matching Independent Component Analysis (SMICA). They have associated these residual structures with the Ophiuchus complex, the Gum nebula, the Orion-Eridanus bubble and the Taurus region. The right-hand plot is the same analysis when the three input maps are cleaned using the WMAP foreground model of Bennett et al. (2003). The residual features are in excellent agreement with those from the middle plot, although the amplitudes are slightly larger, suggesting that the FASTICA template coefficients provide a modestly better cleaning of the WMAP frequency data.

The residual maps from input data cleaned with the K-Ka synchrotron model are shown in the second row of Figure 8. The maps can be compared directly to the equivalent Haslam cases in the row above. It is particularly striking that the residuals are substantially suppressed when using the K-Ka template, especially close to the Galactic Centre. This reinforces the latter’s superiority for foreground separation purposes, although the fact that it is a mixture of physical emission components makes the interpretation of the results more difficult. As before, the residuals are larger when using the WMAP template coefficients, notably so near the Gum nebula – a source of strong free-free emission.

8.2 CMB component

In order to quantify the improvement connected to the iterative processing step, we have studied the CMB components returned by FASTICA when working on the data pre-cleaned with a template analysis stage. They are very similar, as shown in Figure 9. This is also confirmed by the plot of the power spectrum for the CMB map derived from the different cases of the foreground analysis. Figure 10 compares the binned power spectrum of the CMB maps returned from the Q-, V- and W-band

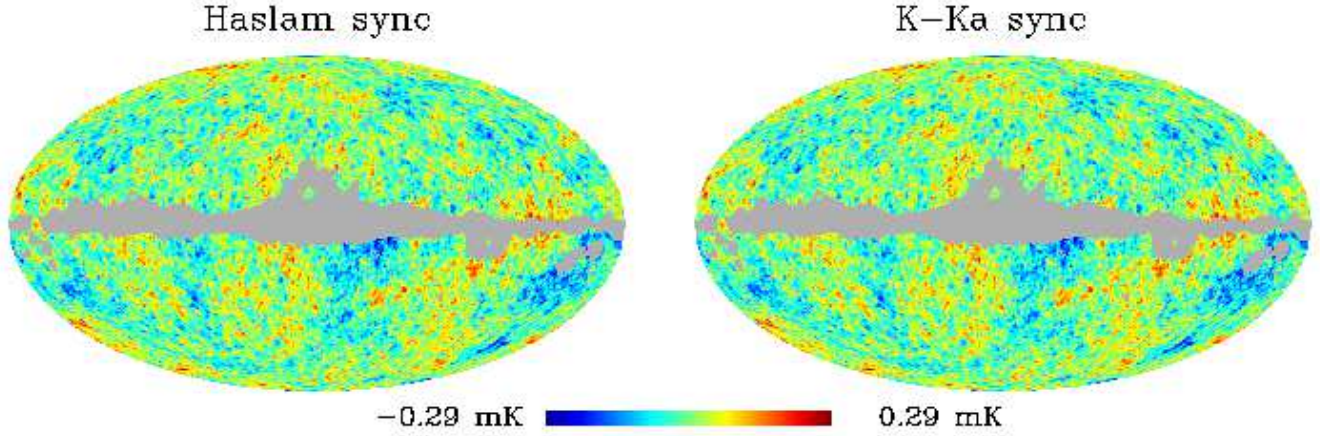


Figure 9. Map of the CMB component obtained by FASTICA with the p -function using WMAP Q -, V - and W -band data pre-cleaned using coupling coefficients estimated with the $Kp2$ mask, and either the Haslam map as the synchrotron template (left) or the K-Ka map (right). The temperature is measured in mK.

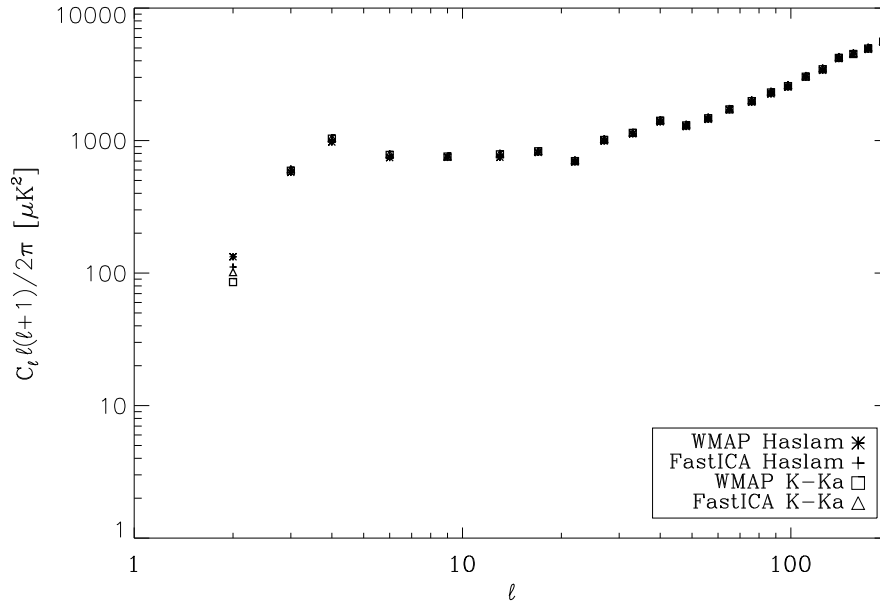


Figure 10. Power spectra of the returned CMB components applying FASTICA to the set of Q -, V - and W -band data from the foreground emissions, using various combinations of foreground templates and fit coefficients.

data cleaned using the coupling coefficients of the FASTICA analysis or the WMAP values, with either the Haslam or K-Ka maps as synchrotron template. The discrepancy is less than $150 \mu K^2$.

Given this, one might argue that the iterative step is unnecessary for WMAP analysis, but we fully expect that it will be essential for studying the *Planck* data in detail. Moreover, in this era of precision cosmology, it is the deviations from the theoretically motivated model spectra which are of interest and the search for evidence of primordial non-Gaussianity requires that false detections due to foreground residuals be eliminated. FASTICA can play a role in the initial cleaning of the data, and then in defining regions on the sky that merit special treatment, be it simply masking them from future cosmological analysis due to the apparently complex nature of the foregrounds there, or the re-application of the component separation techniques on the regions to improve the final CMB sky estimate.

9 DISCUSSION

In this paper, we have utilised a blind component separation algorithm – FASTICA – to address the issue of the Galactic foreground emission in the *WMAP* 3-year data. In particular, we have adapted the technique to allow three Galactic foreground templates (that trace synchrotron, free-free and thermal dust emission) to be fitted to the data on a frequency-by-frequency basis. Specifically, we use the Finkbeiner et al. (2003) $H\alpha$ -map as a template for the free-free emission, the Finkbeiner et al. (1999) FDS8 model for thermal dust emission, and for synchrotron emission two alternatives – the 408 MHz radio continuum all-sky map of Haslam et al. (1982) as utilised in the first year *WMAP* analysis, or the difference of the *WMAP* K- and Ka-band data preferred in their three year analysis.

Detailed simulations indicate that the algorithm behaves in an unbiased way only for two (p, g) of the three non-linear functions typically applied by FASTICA. In these cases, the p -function also appears to be marginally preferred as a consequence of its smaller error bars, both relative to the g -function analysis and the simple χ^2 method that is usually adopted for template fitting.

When applied to the *WMAP* data, we have quantified the foreground contamination in term of coupling coefficients between the data and the foreground templates. The derived values are sensitive to both the extension of the mask applied to exclude the Galactic plane and on the non-linear function used by the algorithm. The mask dependence is likely to reflect genuine variations in the spectral behaviour of the foregrounds with sky location, as seen in previous local studies of template fits by Davies et al. (2006). The non-linear function dependence is plausibly linked to sensitivity to the actual statistical nature of the foreground components (as represented by the templates), and suggests that it may be useful to study more appropriate approximations to the neg-entropy.

We have considered the spectral behaviour of the derived scaling factors when the Haslam et al. (1982) data is used as the synchrotron template. We evaluated the spectral index for the synchrotron emission, the anomalous dust-correlated component, and the free-free emission. In the first two cases, we found steeper, though statistically consistent, spectral behaviour as compared to previous analysis, eg. Davies et al. (2006). For the free-free emission, we confirmed previous observations about inconsistencies in the fitted scaling to convert the $H\alpha$ emissivity to a free-free contribution at K- and Ka-bands. Specifically, the derived factors correspond to thermal electron temperatures of $\sim 4000 K$ compared to the expected value of $8000 K$.

In addition, we find independent verification of a flat spectral dependence in the free-free emissivity as reported by Dobler et al. (2008a). However, this behaviour is seen only for the $Kp2$ sky coverage. With the $Kp0$ mask, the behaviour is even steeper than the expected $\nu^{-2.14}$ dependence, suggesting that the anomalous free-free behaviour is associated with bright structures close the Galactic plane.

We have also proposed that the FASTICA algorithm can be applied ‘iteratively’, that is, used to analyse a set of multi-frequency maps pre-cleaned using templates for which the coefficients have themselves been derived by a FASTICA analysis. This is particularly useful in order to determine the presence of residual foregrounds that arise either due to a mismatch between their spectral dependence and the average high-latitude value determined by the template fits, or because they are new components that are not traced by the adopted templates. In this manner, we have confirmed the existence of a component spatially distributed along the Galactic plane, with pronounced emission near the Galactic center. This is the emission previously noted in the SMICA analysis of Patanchon et al. (2005), and is the ‘*WMAP* haze’ of Finkbeiner et al. (2004). However, the amplitude and extent of the emission is less when the K-Ka map is adopted as the synchrotron template. This is not surprising if the foreground component is a genuinely new contribution to the sky emission that is untraced by the Haslam data. In this context, the K-Ka map must be considered the better template for cleaning the *WMAP* data from foregrounds. However, the interpretation of the results in terms of Galactic emission components is complicated by the fact that the K-Ka template contains a mixture of several, physically distinct, emission mechanisms.

Finally, the analysis that we have performed with the FASTICA algorithm is based on the unrealistic hypothesis that the spectral behaviour of the various foreground emission components is unchanging over the sky. In future work, in order to take into account the spatial variation of the foreground spectra, we will attempt to apply FASTICA on smaller patches of the sky where the assumption of uniform spectral behaviour is more realistic. Given the success of our method in demonstrating the presence of residual foregrounds surviving template-based corrections, we can perhaps utilise the information (ie. the residuals maps) from a near-global approach to identify significant regional spectral variations for such a local analysis.

ACKNOWLEDGMENTS

Some of the results in this paper have been derived using the HEALPix (Górski et al. 2005) package. We acknowledge the use of the Legacy Archive for Microwave Background Data Analysis (LAMBDA). Support for LAMBDA is provided by the NASA Office of Space Science. We acknowledge the use of Craig Markwardt’s fitting package MPFIT⁴.

⁴ <http://cow.physics.wisc.edu/~craigm/idl/fitting.html>

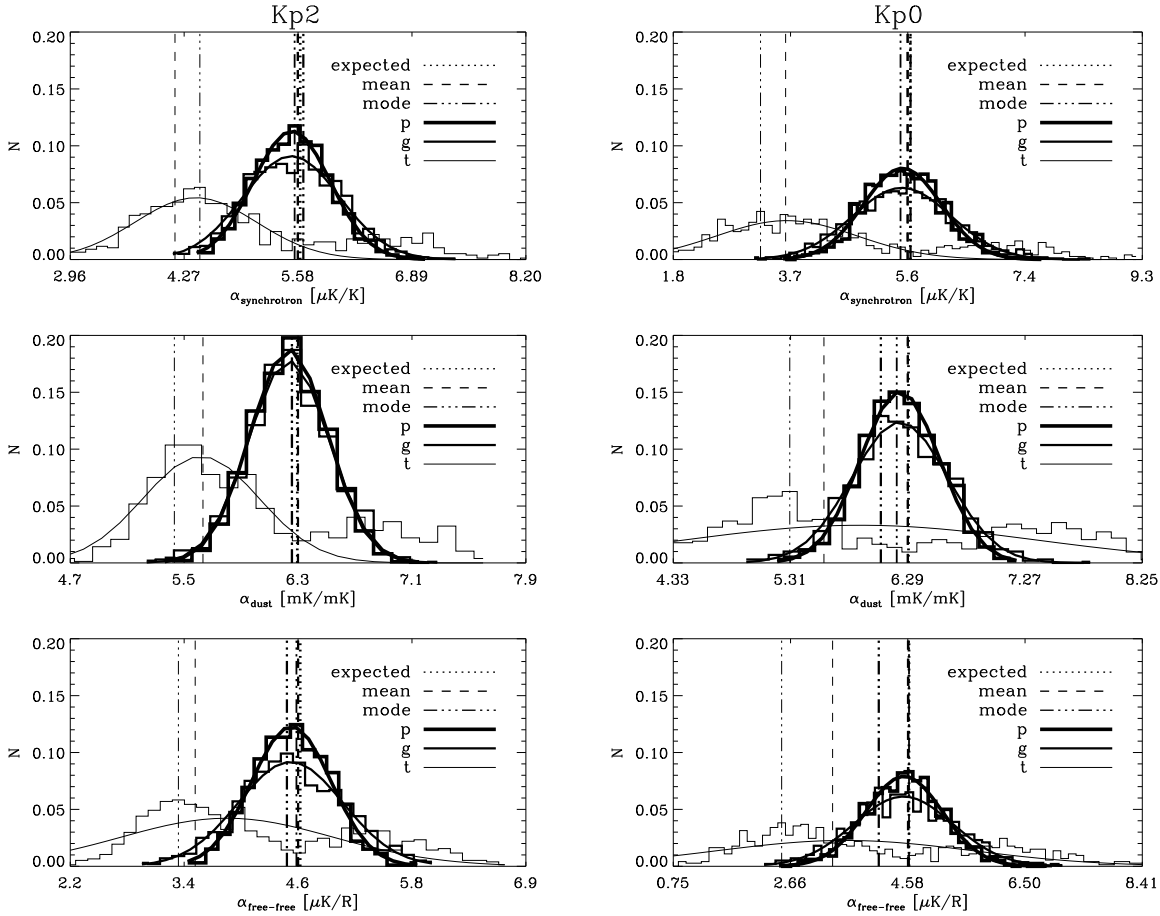


Figure A1. Coupling coefficients distribution determined from simulations of WMAP K-band data with the p -, g - and t -functions. The mean (long-dashes and dashed line), the mode (dash-dot and dash-dot-dot line) and the input values (dotted line) are also shown, together with the best-fit Gaussian profiles.

APPENDIX A:

We have performed 1000 simulations of the microwave sky at each of the 5 WMAP frequencies, each containing a realisation of the CMB signal, the Galactic foreground emission, and instrumental noise appropriate to the specific channel. The study was undertaken at an effective resolution of 1° . Each CMB component corresponds to a Gaussian realisation of the theoretical best fit CMB angular power spectrum with no running spectral index as determined by the WMAP first-year analysis⁵. As verified by Maino et al. (2006) up to $\ell \sim 400$ – the scales of interest for 1° smoothed data – the differences between the 3 year and 1 year best-fit models are less than 1.5% and therefore not expected to bias the results significantly. The white noise component is simulated for each of the 10 DAs in the usual manner. That is, for a given pixel a Gaussian random number is selected with zero mean and a variance corresponding to the ratio of the noise variance per observation for that channel and the number of observations for the pixel in question. The CMB component and noise realisations are then combined, and the maps smoothed. For those frequencies with multiple associated DAs, the band averaged skymaps are formed using simple averaging. For the foreground emission, we added to each simulated frequency map three Galactic templates as described in section 3, appropriately scaled to the frequency in question. These maps were then used as input data for FASTICA.

As a convenient point of reference for our FASTICA results, we have also included a simple template fitting analysis. In general, the correlation method can be extended to include various constraints on the data, eg. fixed dust or free-free spectral indices. This is the case described by Hinshaw et al. (2007) in the analysis of the 3 year data of WMAP but we impose no such constraints here. The best-fit monopole is removed from each of the sky maps before computing the coefficients, to be consistent with the FASTICA approach.

Using these simulations, we can determine the suitability of the non-quadratic functions adopted in the FASTICA analysis

⁵ http://lambda.gsfc.nasa.gov/data/map/powspec/wmap_lcdm_pl_model_yr1_v1.txt

for template fitting. Figure A1 summarises the situation when using the Haslam 408 MHz sky map as a tracer of the synchrotron emission. The templates were scaled using the weights from Table 3 of Bennett et al. (2003), where for the Q-, V- and W- bands we have considered the average values.

The distribution of coefficients determined by FASTICA when utilising the t function is clearly unsatisfactory – the distribution is not Gaussian and has broad asymmetric tails, and is strongly biased away from the input values. In the case of the Kp0 mask, the distribution also shows evidence of bimodality, and for many simulations the FASTICA analysis does not even converge. We conclude that, when using the t function FASTICA is unable to distinguish Galactic emission in the *WMAP* data as described by template maps, and we do not include results based on this non-quadratic function for the analysis of the real data.

In contrast, the behaviour of the p and g functions for determining the coupling coefficients seems to be suitable for our purposes. Although we show results only for the K-band simulations, we find that at all frequencies the scaling factors are very well described by Gaussian distributions – in fact the corresponding measures of the skewness and kurtosis values are small in all cases. The mean values for the simulated distributions of coefficients are very similar to the inputs, and there is no evidence of significant bias. This is true also for the mode if we consider p , but with g the mode is slightly smaller than the input value for the dust and free-free emission: indeed, it could explain partially the difference between the coefficients obtained in the real analysis. However, the main difference between the two functions is that the distribution determined with g is broader than with the p function: corresponding to a larger statistical uncertainty for analyses made with the former.

It is likely that some of the performance features of the different non-linear functions are related to the statistical features of the physical emission as traced by the template sky maps. Not surprisingly, the results indicate that the template fits using FASTICA are sensitive to the extent of the mask applied to the data. For a narrower Galactic exclusion region, the template fits have smaller errors. This is certainly in part due to simple ‘sample variance’ type arguments, but may also be connected with the degree to which bright foreground emission near to the applied cut can stabilise the fits. Variations in the fitted amplitudes of the foreground components against the observed data as a function of mask may also reveal genuine changes in the physical properties and spectral behaviour of the foregrounds with latitude.

In Figure A2 we have plotted the fitted Q-band amplitudes for one template against another for the various template permutations in order to study the significance of cross-talk between the maps. There is an apparent anti-correlation between the synchrotron and the dust coefficients (as specified by the linear correlation coefficient r), but no clear evidence for such behaviour between synchrotron and free-free or free-free and dust. This behaviour is essentially identical for all of the *WMAP* frequencies. Some care should then be exercised in interpreting the coefficients for the former two components.

We have repeated the simulations and analysis using the *WMAP* K-Ka map as the synchrotron template, in this case only for the Q-, V- and W-bands. The templates were scaled using the coefficients from Hinshaw et al. (2007), but adopting the mean of the coefficients over the differencing assemblies. The distributions of the coefficients are again symmetric and well fitted by Gaussians as in the case of the Haslam template. Furthermore, the results are consistent with the previous ones concerning the dependence of the coefficients on the FASTICA functions. The analogous scatter plots between pairs of coefficients are shown in Figure A3. This time, the synchrotron coefficients are anti-correlated with the free-free results. Indeed, this should be expected since the template must contain both synchrotron and free-free emission. However, the synchrotron coefficients are more strongly anti-correlated with the dust values, which is easily interpreted as being due to the presence of anomalous dust correlated emission in the K-Ka template. This factor is not taken into account by Hinshaw et al. (2007) in their constrained template analysis.

Finally, we performed the same statistical study with the simple χ^2 minimisation in order to compare the performances of the two methods. The results depend on the template considered. For the synchrotron and free-free emission, the uncertainties are larger than the FASTICA values obtained with either the p - or g -function, substantially so in the former case. For the dust emission they are essentially equivalent. It is therefore clear that FASTICA is a reliable method to perform template fitting, in some cases outperforming the conventional χ^2 minimisation. This is particularly true for p , and we could conclude that it is the most stable non-linear function, although this is not a definitive argument. Figure A4 shows scatter plots between pairs of recovered Q-band coefficients when using either the Haslam or K-Ka maps as synchrotron templates. It is interesting to note that there is a hint of anti-correlation between the synchrotron and free-free coefficients using the Haslam template, but that this becomes significant when the K-Ka template is employed. Moreover, a significant correlation between free-free and dust is seen in the latter case. The simple χ^2 method appears to demonstrate more cross-talk between the coefficients of the different components than seen for the FASTICA analysis. This may help to understand some of the differences seen in the results obtained with the observed data.

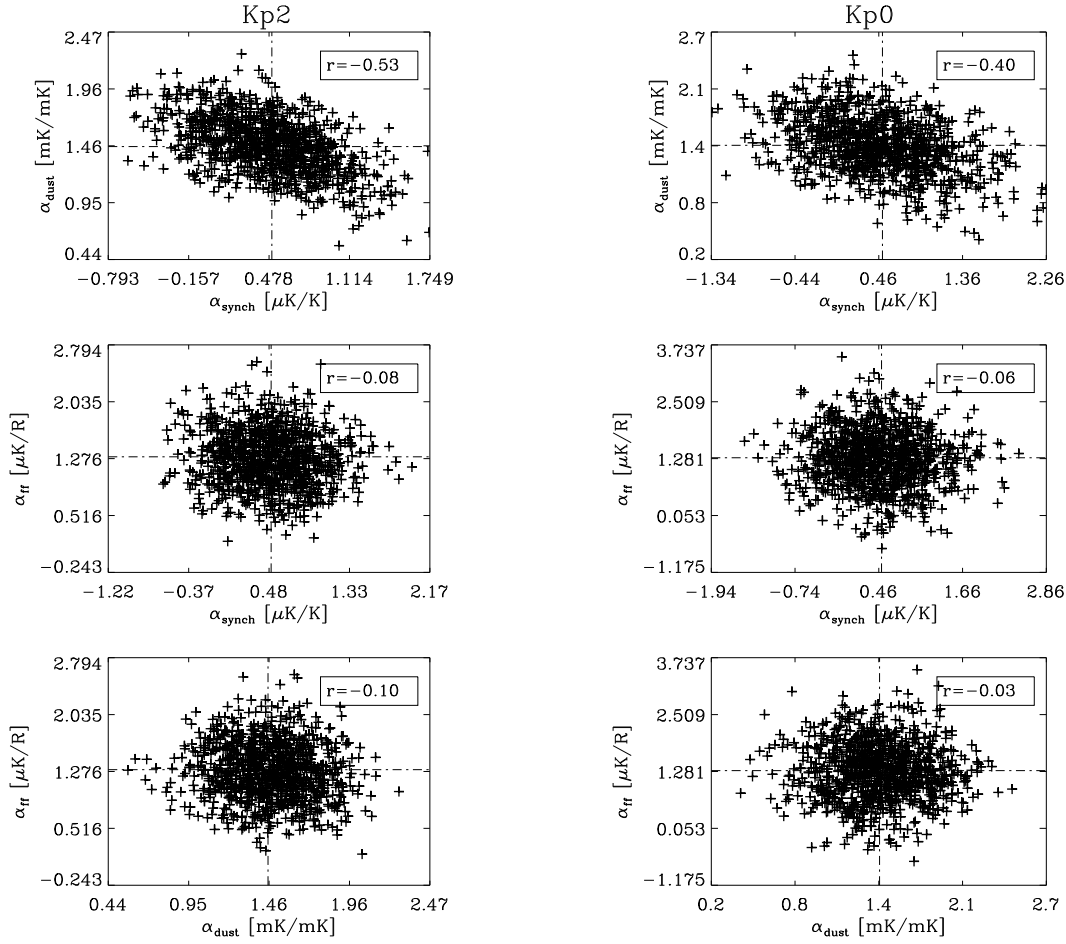


Figure A2. Scatter plots of the coupling coefficients obtained by FASTICA with the p -function using the simulations performed using the Haslam map as synchrotron template. We show as an example the results in the Q-band. There is very little change in the correlation properties as a function of frequency.

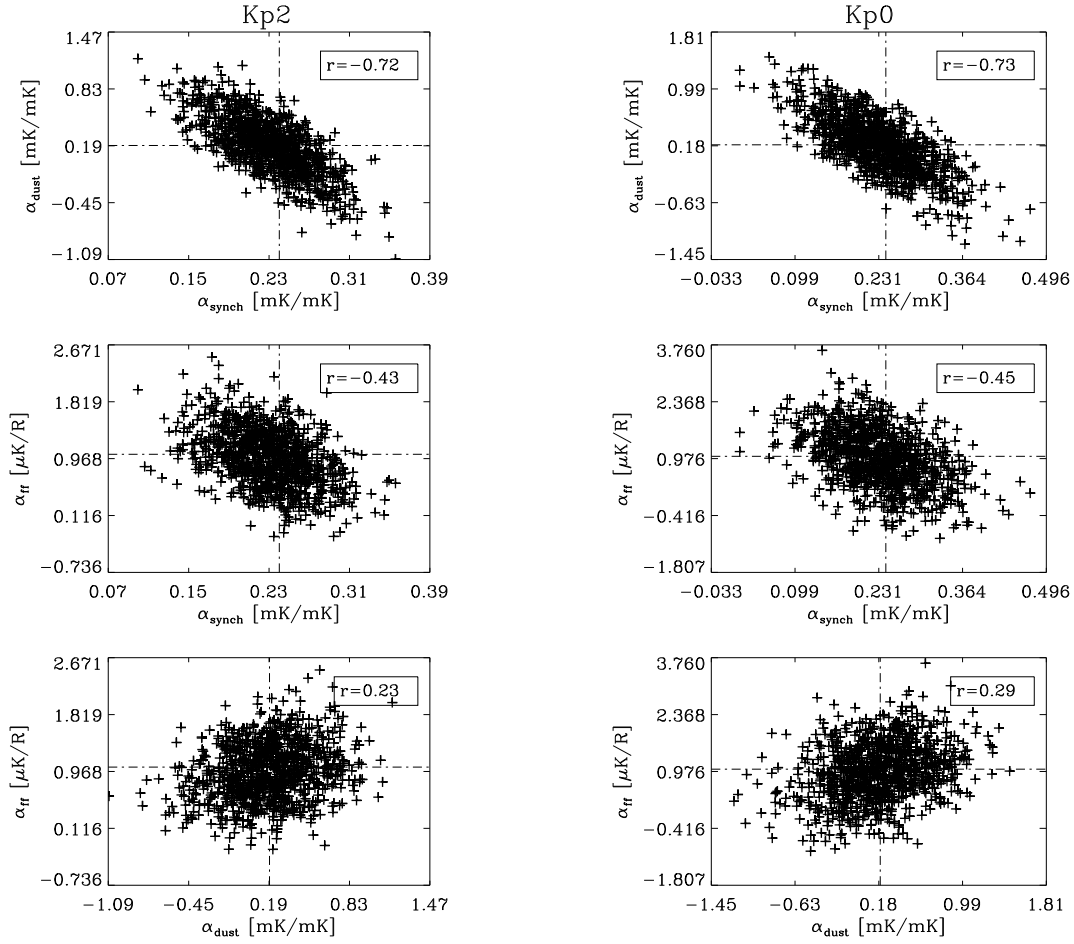


Figure A3. Scatter plots of the coupling coefficients obtained by FASTICA with the p -function using the simulations performed with the K - K_a map as synchrotron template. We show as an example the results in the Q -band. There is very little change in the correlation properties as a function of frequency.

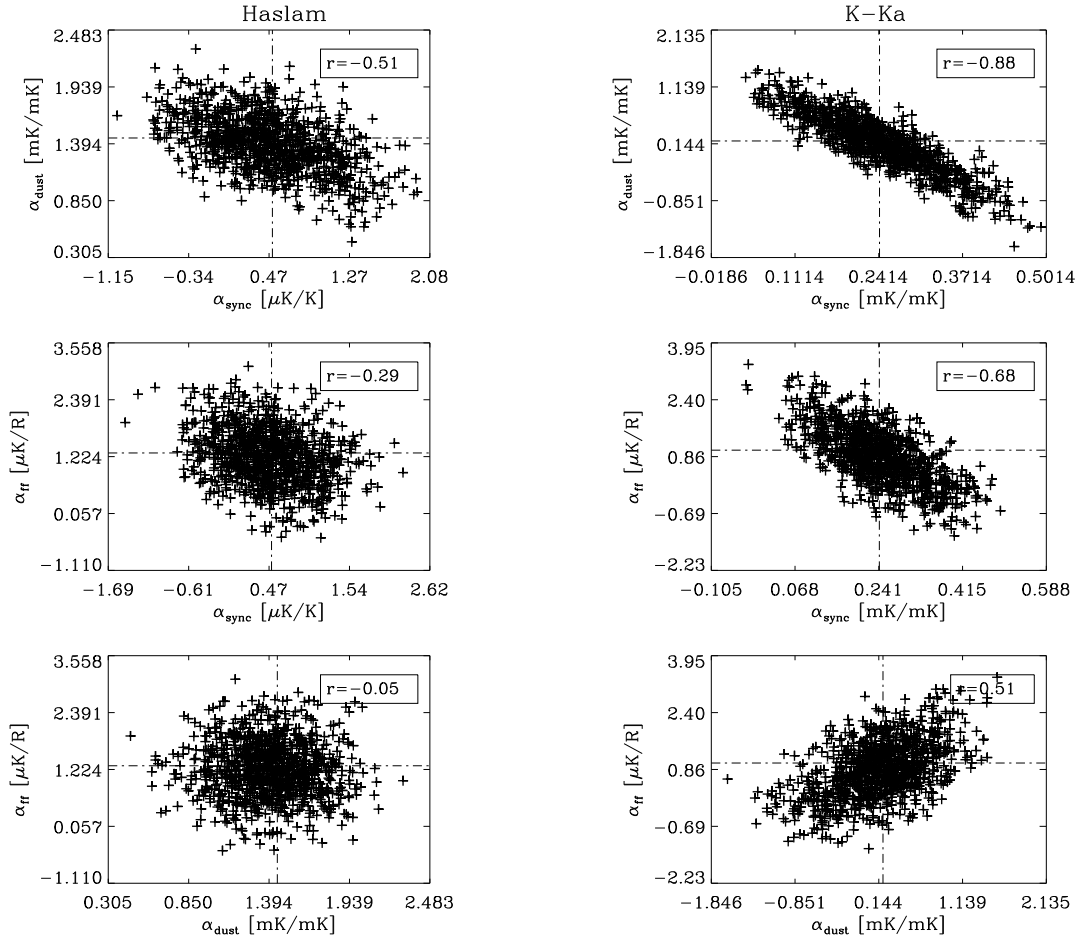


Figure A4. Scatter plots of the scaling factors obtained via the simple χ^2 method on Kp2 sky coverage with simulations performed using either the Haslam map (left column) or the K-Ka map (right column) as the synchrotron template. We show as an example the results in the Q-band. There is very little change in the correlation properties as a function of frequency.

REFERENCES

- Baccigalupi, C. et al. , 2004, *MNRAS* , 354, 55
- Banday A.J. et al. , 2003, *MNRAS* , 345, 897
- Bennett C.L. et al. , 2003, *Astrophys. J. Supp.* , 148, 97
- Bonaldi, A., Ricciardi, S., Leach, S., Stivoli, F., Baccigalupi, C., de Zotti, G., 2007, *MNRAS* , 382, 1791
- Casassus S., Readhead A.C.S., Pearson T.J., Nyman L.-Å., Shepherd M.C., & Bronfman L. 2004, *Astrophys. J.* , 603, 599
- Davies R. D., Watson, R. A., Gutierrez, C. M., 1996, *MNRAS* , 278, 925
- Davies R.D., Dickinson C., Banday A.J., Jaffe T.R., Górski K.M., Davis R.J., 2006, *MNRAS* 370, 1125
- de Oliveira-Costa A., Tegmark M., Page L., & Boughn S. 1998, *Astrophys. J.* , 509, L9
- Dennison B., Simonetti J.H., Topasna G.A., 1998, *PASP*, 15, 147
- Dickinson C., Davies R.D., Davis R.J., 2003, *MNRAS* , 341, 369
- Dobler, G., Finkbeiner D.P., 2008, *Astrophys. J.* , submitted
- Dobler, G., Finkbeiner D.P., 2008, *Astrophys. J.* , submitted
- Draine B.T., Lazarian A., 1998a, *ApJ*, 494, L19
- Draine B.T., Lazarian A., 1998b, *ApJ*, 508, 157
- Eriksen, H. K., Dickinson, C., Lawrence, C. R., Baccigalupi, C., Banday, A. J., Górski, K. M., Hansen, F. K., Pierpaoli, E., Seiffert, M. D., 2006, *New Astronomy Reviews*, 50, 861
- Finkbeiner D.P., Davis, M., Schlegel D.J., 1999, *Astrophys. J.* , 524, 867
- Finkbeiner D.P., Schlegel D.J., Frank C., & Heiles C. 2002, *Astrophys. J.* , 566, 898
- Finkbeiner D.P., 2003, *Astrophys. J. Supp.* , 146, 407
- Finkbeiner D.P., 2004, *Astrophys. J.* , 614, 186
- Gaustad J.E., McCullough P.R., Rosing W., Van Buren D., 2001, *PASP*, 113, 1326
- Górski, K.M., Hivon, E., Banday, A.J., Wandelt, B.D., Hansen, F.K., Reinecke, M., & Bartelmann, M., 2005, *Astrophys. J.* , 622, 759
- Haffner L.M., Reynolds R.J., Tuft S.L., Madsen G.J., Jaehnig K.P., Percival J.W., 2003, *ApJS*, 149, 405
- Hansen, F.K., Banday, A.J., Eriksen, H.K., Górski, K.M., Lilje, P.B., 2006, *Astrophys. J.* , 648, 784
- Haslam C.G.T. et al. , 1982, *Astron. & Astrophys. Suppl.* , 47, 1
- Hyvärinen A., 1999, *IEEE Signal Processing Lett.* , 6, 145
- Hyvärinen A. & Oja E., 2000, *Neural Networks* , 13, 411
- Hinshaw G. et al. , 2007, *Astrophys. J. Supp.* , 170, 288
- Hivon, E., Górski, K.M., Netterfield, B., Crill, B.P., Prunet, S.P., & Hansen, F.K., 2002, *Astrophys. J.* , 567, 2
- Kogut A., Banday A.J., Bennett C.L., Górski K.M., Hinshaw G., & Reach W.T. 1996a, *Astrophys. J.* , 460, 1
- Kogut A., Banday A.J., Bennett C.L., Górski K.M., Hinshaw G., Smoot G.F., & Wright E.I. 1996b, *Astrophys. J. Lett.* , 464, L5
- Leitch E.M., Readhead A.C.S., Pearson, T.J., & Myers, S.T., 1997, *Astrophys. J. Lett.* , 486, L23
- Maino D. et al. , 2002, *MNRAS* , 334, 53
- Maino D., Banday A.J., Baccigalupi C., Perrotta F., Górski K.M., 2003, *MNRAS* , 344, 544
- Maino D., Donzelli S., Banday A.J., Stivoli F., Baccigalupi C., 2006, *MNRAS*
- Park, C.-G. Park, C. Gott, J. R., 2007, *Astrophys. J.* , 660, 959
- Patachon G., Cardoso J.F., Delabrouille, J., Vielva P., 2005, *MNRAS* , 364, 1185
- Reich, P., Reich, W., 1988, *A&A*, 196, 211
- Schlegel, D. J., Finkbeiner, D. P. Davis, M., 1998, *Astrophys. J.* , 500, 525
- Tegmark, M., de Oliveira-Costa, A., Hamilton, A. J., 2003, *PRD*, 68, 123523